Boundary Layer and Shallow Cumulus Clouds in a Medium-Range Forecast of a Large-Scale Weather System

STÉPHANE BÉLAIR, JOCELYN MAILHOT, CLAUDE GIRARD, AND PAUL VAILLANCOURT

Meteorological Research Branch, Meteorological Service of Canada, Dorval, Quebec, Canada

(Manuscript received 2 February 2004, in final form 17 December 2004)

ABSTRACT

The role and impact that boundary layer and shallow cumulus clouds have on the medium-range forecast of a large-scale weather system is discussed in this study. A mesoscale version of the Global Environmental Multiscale (GEM) atmospheric model is used to produce a 5-day numerical forecast of a midlatitude large-scale weather system that occurred over the Pacific Ocean during February 2003. In this version of GEM, four different schemes are used to represent (i) boundary layer clouds (including stratus, stratocumulus, and small cumulus clouds), (ii) shallow cumulus clouds (overshooting cumulus), (iii) deep convection, and (iv) nonconvective clouds. Two of these schemes, that is, the so-called MoisTKE and Kuo Transient schemes for boundary layer and overshooting cumulus clouds, respectively, have been recently introduced in GEM and are described in more detail.

The results show that GEM, with this new cloud package, is able to represent the wide variety of clouds observed in association with the large-scale weather system. In particular, it is found that the Kuo Transient scheme is mostly responsible for the shallow/intermediate cumulus clouds in the rear portion of the large-scale system, whereas MoisTKE produces the low-level stratocumulus clouds ahead of the system. Several diagnostics for the rear portion of the system reveal that the role of MoisTKE is mainly to increase the vertical transport (diffusion) associated with the boundary layer clouds, while Kuo Transient is acting in a manner more consistent with convective stabilization. As a consequence, MoisTKE is not able to remove the low-level shallow cloud layer that is incorrectly produced by the GEM nonconvective condensation scheme. Kuo Transient, in contrast, led to a significant reduction of these nonconvective clouds, in better agreement with satellite observations. This improved representation of stratocumulus and cumulus clouds does not have a large impact on the overall sea level pressure patterns of the large-scale weather system. Precipitation in the rear portion of the system, however, is found to be smoother when MoisTKE is used, and significantly less when the Kuo Transient scheme is switched on.

1. Introduction

Close examination of today's satellite imagery reveals, in a daily manner, just how much of earth's surface (especially oceans) is covered with stratocumulus (Sc) and shallow cumulus (Cu) clouds. Because of the important role they are believed to play in the climate system, and because of the effect they have on local weather, Sc clouds have been extensively studied in the last few decades (see reviews by Stull 1988; Driedonks and Duynkerke 1989) and are still the subject of large program studies (Brenguier et al. 2000; Stevens et al. 2003). In addition to their radiative impacts, these clouds modulate turbulent mixing near the top of the atmospheric boundary layer (ABL). The existence and maintenance of Sc clouds depend on the equilibrium between many physical processes, including heat and moisture supply from the surface, cloud-top radiative cooling (Randall 1980a; Slingo et al. 1982a; Nicholls 1984), cloud-top entrainment (Deardorff 1980; Randall 1980b, 1984; Stevens 2002), daytime solar warming of the cloudy air (Slingo et al. 1982b; Bougeault 1985a), cloud microphysics (Austin et al. 1995; Duynkerke et al. 1995; Stevens et al. 1998), and large-scale subsidence.

The role of Cu clouds is similar to that of Sc clouds in the sense that they also increase the turbulent transport of heat and moisture from the ABL to the free atmosphere (Stull 1985; Wang and Lenschow 1995; Cuijpers

Corresponding author address: Stéphane Bélair, Recherche en Prévision Numérique, Meteorological Service of Canada, 2121 Trans-Canada Highway, Room 500, Dorval QC H9P 1J3, Canada. E-mail: stephane.belair@ec.gc.ca

Unauthenticated | Downloaded 08/13/24 05:34 PM UTC

et al. 1996). In contrast with Sc clouds, however, they are more scattered, more intermittent, and may penetrate a few kilometers into the free atmosphere above the ABL (Austin et al. 1985; de Roode and Duynkerke 1997). The main properties of Cu clouds (e.g., coverage fraction, depth, updraft velocity) greatly depend on entrainment processes, which control the dilution of the convective updrafts by mixing with environmental air. These entrainment processes are much debated, as evidence suggests that both vertical and horizontal mixing may play important roles (Taylor and Baker 1991; Blyth 1993; Siebesma 1998). Shallow cumulus clouds are often found in transition regions between Sc and deep convective clouds where large-scale subsidence is gradually relaxed. The so-called trade wind cumuli, for instance, are observed in the subtropical belts between the upward and downward branches of the Hadley cell (Riehl et al. 1951; Malkus 1954).

The mixing associated with Sc and Cu clouds is included in atmospheric models using either a moist turbulence scheme or a mass-flux approach. In the first approach, Sc and Cu cloud activity is represented by vertical diffusion (mixing) produced by the ABL turbulence scheme. In mass-flux schemes, entraining/detraining plume models provide the vertical mixing associated with Cu clouds (Tiedtke 1989; von Salzen and McFarlane 2002; Deng et al. 2003). Mass-flux schemes may not be adequate for representing more stable clouds such as stratus layers near the top of the ABL. For this reason, they are normally used in combination with other representations of convectively less active clouds. For example, a prognostic scheme for neutrally buoyant clouds was introduced in Deng et al. (2003) to complement their mass-flux scheme. In Tiedtke (1993), a cloud cover scheme of a similar nature is also used for the same purpose.

The clouds properties, that is, subgrid cloud fraction and water content, can be determined using different methods: empirical diagnostic methods (e.g., Slingo 1987), prognostic equations for cloud water but still diagnostic for cloud fraction (e.g., Sundqvist 1993), prognostic equations for both cloud water and cloud fraction (e.g., Tiedtke 1993), or using a statistical approach (e.g., Sommeria and Deardorff 1977; Bougeault 1981, 1985a). The last technique is of particular interest in the context of low-order turbulence closure models that are now widely utilized in the atmospheric modeling community. In this approach, Sc and small Cu cloud activity have the effect of increasing the vertical diffusion (mixing) produced by the ABL turbulence scheme. Duynkerke and Driedonks (1987, 1988) and Bechtold et al. (1992) have successfully reproduced the main features of Sc clouds with this strategy. Bechtold et al. (1995) modified the distribution function used for subgrid-scale clouds in order to also consider very shallow Cu clouds (see also Bechtold and Siebesma 1998). More recently, Chaboureau and Bechtold (2002) even extended this approach to all types of clouds, including deep convection.

Our aim in this study is to examine the representation of clouds, with particular attention to boundary layer and shallow cumulus clouds, in the context of medium-range weather forecasts using a global uniform resolution model. As described in the next section, four different schemes are used in this study to represent a range as wide as possible of clouds. These four schemes are for boundary layer clouds (MoisTKE scheme), overshooting shallow cumulus (Kuo Transient scheme), deep convection (Kain and Fritsch 1990, 1993), and nonconvective clouds (Sundqvist 1978; Pudykiewicz et al. 1992). The first two schemes, which are new, are described in the next section.

There is no a priori correct number of cloud schemes that have to be used to represent clouds in an atmospheric model. This number depends on the particular schemes that are included in the atmospheric model, and on the configuration or application in which the model is integrated. For instance, a meso-γ-scale model (grid size of about 1 km) does not need to include a representation of deep convection, but certainly requires a grid-scale condensation scheme and even an implicit representation of boundary layer clouds. In a large-eddy simulation (LES) approach (grid size of about 10–50 m), many only use a cloud microphysics scheme, although some also include statistical cloud schemes (assuming Gaussian distributions) for resolutions of tens of meters (Sommeria 1976; Chlond 1992; Lewellen et al. 1996). For global medium-range weather forecasting with grid sizes on the order of 30–35 km, the combination of four schemes presented in this work will be shown to lead to a realistic representation of the wide range of clouds that were observed during a large-scale weather event over the Pacific. Of course, it is not excluded that in other atmospheric models, in which different cloud schemes are available, this could not be possible using a smaller number of schemes.

Although many efforts are currently under way to unify the representation of low-level convective clouds (e.g., Bechtold et al. 1995; Lappen and Randall 2001; Golaz et al. 2002), we have chosen to use two different schemes for the low-level boundary layer (very shallow) clouds and the more penetrative small cumulus (overshooting Cu). This approach was made necessary because of the many problems that appeared in the extensive tests that were conducted to determine the

Unauthenticated | Downloaded 08/13/24 05:34 PM UTC

optimal configuration of the next regional (short range) and global (medium range) deterministic forecast models to be implemented operationally at the Canadian Meteorological Centre (CMC). In these tests, the chief problems that were observed were the lack of penetrative cumulus clouds produced by the model and the balance between convective and nonconvective precipitation (which is in part controlled by the small and intermediate cumulus activity, as will be shown). Several cloud schemes were examined and tested [shallow version of Kain and Fritsch (1990, 1993); von Salzen and McFarlane (2002), MoisTKE alone, Kuo Transient alone], but none were able to improve the results as convincingly as what is shown below with the combination of MoisTKE and Kuo Transient. Although some overlap exists between these two schemes (potential double counting is avoided by using a sequential treatment of clouds, in which the second scheme sees an environment already modified by the first), the clouds they produced have different vertical extensions because of the main assumptions on which these schemes are based.

Others have used approaches similar to the one presented in this study, that is, with two different schemes to represent boundary layer clouds and overshooting Cu. For instance, it is admitted in Tiedtke (1989) that the cumulus scheme is not able to represent very shallow, that is, PBL, clouds; in Teixeira and Hogan (2002), a diagnostic cloud scheme was used for cumulus clouds and a statistical scheme for stratocumulus; in Deng et al. (2003), two different approaches were used for cumulus and what they called the neutrally buoyant clouds.

Our main objectives are thus to (i) determine how accurately Sc and Cu clouds are represented in a 5-day weather forecast of a synoptic-scale weather system that occurred over the Pacific Ocean in February 2003, (ii) discuss the specific role and importance of the Sc and Cu cloud schemes, and (iii) show how Sc and Cu clouds interact with deep convection and influence the evolution of the large-scale weather system.

2. Atmospheric modeling system

The results presented in this study were obtained with the Global Environmental Multiscale model (GEM; Côté et al. 1998a,b), now used operationally for short-, medium-, and long-range weather forecasting at the CMC. In our version of GEM, the primitive hydrostatic equations are integrated on a global 800×600 grid with a uniform resolution of 0.45° in longitude and 0.30° in latitude (i.e., about 33 km at 50° latitude). The resolution is varying in the vertical, with a total of 58 levels extending up to 10 hPa. Many of these levels are located in the lowest 2 km (spacing between levels of about 250 m at 2 km above the surface) and near the tropopause (spacing of about 250 m near 150 hPa). More details about GEM's numerics and dynamics are given in Table 1.

In addition to the schemes described below for Sc and Cu clouds, a complete set of physical parameterizations is included in GEM, with (a) solar and infrared radiation fully interactive with clouds (Fouquart and Bonnel 1980; Garand 1983); (b) surface fluxes of heat, moisture, and momentum over four types of surfaces (land, water, sea ice, and glaciers; see Bélair et al. 2003a,b); (c) implicit vertical diffusion with prognostic turbulent kinetic energy (TKE) and a mixing length based on Bougeault and Lacarrère (1989; see Benoit et al. 1989; Bélair et al. 1999); (d) deep convection using the Kain and Fritsch (1990, 1993) scheme; and (e) nonconvective clouds based on Sundqvist (1978; see also Pudykiewicz et al. 1992).

a. The MoisTKE boundary layer cloud scheme

A unified cloudiness–turbulence scheme has been recently included in GEM, based on the work of Bechtold

TABLE 1. Summary of the GEM forecast system.

Dynamics/numerics
• Hydrostatic primitive equations;
• Global uniform resolution of 0.45° longitude and 0.30° latitude (800×600);
• Variable vertical resolution with 58 levels; model top at 10 hPa;
• Time step of 900 s (i.e., 15 min);
• Cell-integrated finite-element discretization on Arakawa C grid;
• Terrain-following hydrostatic pressure vertical coordinate;
• Two-time-level semi-implicit time scheme;
• 3D semi-Lagrangian advection;
• ∇^6 horizontal diffusion on momentum variables; increased horizontal diffusion (sponge) for the four uppermost levels;
• Periodic horizontal boundary conditions;
• No motion across the lower and upper boundaries.
Physics
• Planetary boundary layer based on TKE with statistical representation of subgrid-scale cloudiness (MoisTKE);
• Fully implicit vertical diffusion;
• Stratified surface layer, distinct roughness lengths for momentum and heat/humidity;
• Four types of surface represented: land, water, sea ice, and glaciers;
• Solar/infrared radiation schemes with cloud-radiation interactions based on predicted cloud radiative properties;
• Kuo Transient scheme for shallow convection;
• Kain–Fritsch scheme for deep convection;
• Sundqvist scheme for nonconvective condensation.

Unauthenticated | Downloaded 08/13/24 05:34 PM UTC

and collaborators (see Bechtold et al. 1992, 1995; Cuijpers and Bechtold 1995; Bechtold and Siebesma 1998). In our implementation of this technique (hereafter referred to as MoisTKE; see Mailhot and Bélair 2002), the vertical diffusion associated with boundary layer turbulence is done on the conservative thermodynamic variables θ_{il} and q_w representing ice–liquid potential temperature and total water content, respectively. The vertical diffusion is then performed using

$$\frac{\partial \theta_{il}}{\partial t} = \frac{1}{\rho}\left[\frac{\partial}{\partial z}\rho K_T\left(\frac{\partial \theta_{il}}{\partial z}\right)\right]; \quad \frac{\partial q_w}{\partial t} = \frac{1}{\rho}\left[\frac{\partial}{\partial z}\rho K_T\left(\frac{\partial q_w}{\partial z}\right)\right], \tag{1}$$

in which θ_{il} and q_w are defined the following way:

$$\theta_{il} = \theta\left(1 - \frac{Lq_c}{c_p T}\right); \quad q_w = q_c + q_v. \tag{2}$$

In these equations, θ is the potential temperature, T is the temperature, q_v is the water vapor content, q_c is the total cloud water content composed of liquid and ice water contents (q_l and q_i), K_T is the eddy diffusivity coefficient for temperature/humidity computed from TKE and a turbulent mixing length, c_p is the specific heat of air at constant pressure, and $L = L_v + fL_f$ is the latent heat factor, in which L_v and L_f are latent heats of vaporization and fusion, respectively, and f is the ice fraction of the cloud condensate, set equal to zero at temperatures above −15°C, to unity at temperatures lower than −25°C, and with a linear variation between −25° and −15°C.

Following Bechtold's approach, the mixing effect of boundary layer clouds is represented through the buoyancy flux ($F_{\theta_v} = \overline{w'\theta_v'}$), which is an important production term for TKE. By expressing the turbulent flux of total cloud water q_c as $F_{q_c} = N f_N F_s$ (see Cuijpers and Bechtold 1995) in which N is the subgrid-scale cloud fraction, f_N is a nondimensional flux enhancement factor, and F_s is a supersaturation flux [$s = q_w - q_{sat}(T)$, where $q_{sat}(T)$ is specific humidity at saturation], the buoyancy flux may be written as a combination of the two conservative variables fluxes:

$$F_{\theta_v} = (1 + 0.61\, q_w - \beta\, b\, f_N N)F_{0_{il}} + (\alpha + \beta\, a\, f_N N)F_{q_w}, \tag{3}$$

in which the thermodynamic coefficients a, b, α, and β are given by

$$a = (1 + Lq_{sl,T}/c_p)^{-1}; \quad b = a(T/\theta)q_{sl,T}; \tag{4}$$

$$\alpha = 0.61\,\theta; \quad \beta = (\theta/T)(L/c_p) - 1.61\,\theta; \tag{5}$$

where $q_{sl,T} = L\, q_{sat}(T_l)/R_v T_l^2$ with $T_l = \theta_l(T/\theta)$, and R_v is the gas constant for water vapor.

Statistical relations appropriate to the various boundary layer cloud regimes, based on observations and large-eddy simulations, were used to define N, q_c, and f_N. These relations are function of a single parameter Q_1 representing a normalized measure of saturation, that is, $Q_1 = s/\sigma_s$, where σ_s is the standard deviation of s. They correspond to a slight modification to the original relations of Bechtold and Siebesma (1998) that give a better fit to the data of their Fig. 4 for the product $f_N N$. For the subgrid-scale cloud fraction N:

$$N = \max\{0, \min[1, 0.5 + 0.36 \arctan(1.55\, Q_1)]\}, \tag{6}$$

for the total cloud water content q_c:

$$\frac{q_c}{\sigma_s} = e^{-1} + 0.66\, Q_1 + 0.086\, Q_1^2 \quad \text{if} \quad Q_1 \geq 0$$

$$\frac{q_c}{\sigma_s} = e^{1.2Q_1 - 1} \quad \text{if} \quad Q_1 < 0; \tag{7}$$

and for the flux enhancement factor f_N:

$$\begin{aligned} f_N &= 1 && \text{if} \quad Q_1 \geq 1 \\ f_N &= e^{-0.3(Q_1-1)} && \text{if} \quad -1.7 \leq Q_1 < 1 \\ f_N &= e^{-2.9(Q_1+1.4)} && \text{if} \quad -2.4 \leq Q_1 < -1.7 \\ f_N &= 0.60/N && \text{if} \quad -4.0 \leq Q_1 < -2.4 \\ f_N &= 0.30(Q_1 + 6)/N && \text{if} \quad -6.0 \leq Q_1 < -4.0. \end{aligned} \tag{8}$$

It is worth noting from these statistical relations that the product $f_N N$ is well described by the Gaussian approximation (i.e., $f_N \approx 1$) for $Q_1 > -1.5$, representative of Sc clouds. For smaller values of Q_1 (< -2), the flux enhancement factor is dramatically increased because of the representation of small Cu clouds. These characteristics of Bechtold's subgrid-scale cloudiness scheme are well conveyed by Fig. 4 of Bechtold and Siebesma (1998), which shows f_N and the product $f_N N$ as a function of the parameter Q_1.

b. The Kuo Transient shallow convection scheme

Several variations of the Kuo scheme for deep convection (Kuo 1965, 1974; Anthes 1977) have been developed and tested by Girard and his colleagues (see Mailhot et al. 1998). One of these modified versions, the Kuo Transient scheme, was specifically made to represent overshooting Cu activity.

In Kuo Transient, grid-scale variables are written as linear combinations of their in-cloud and environmental values:

Unauthenticated | Downloaded 08/13/24 05:34 PM UTC

$$x = (1 - N_{\mathrm{KT}})x_e + N_{\mathrm{KT}}x_c, \tag{9}$$

in which x either represents the temperature T or the specific humidity q_v, N_{KT} is the cloud fraction, and the subscripts c and e are for cloudy and environmental air, respectively. The temperature and humidity tendencies are obtained by differentiating (9):

$$\frac{\partial x}{\partial t} = (1 - N_{\mathrm{KT}})\frac{\partial x_e}{\partial t} + N_{\mathrm{KT}}\frac{\partial x_c}{\partial t} + (x_c - x_e)\frac{\partial N_{\mathrm{KT}}}{\partial t}. \tag{10}$$

Assuming that the shallow cumulus clouds are quasi-stationary (i.e., $\partial x_c/\partial t \approx 0$) and that the environment is in quasiequilibrium, that is, that radiative cooling approximately compensates warming due to subsidence ($\partial x_e/\partial t \approx 0$), the cumulus parameterization can be expressed in the following manner:

$$\frac{\partial x}{\partial t} = \left(\frac{x_c - x}{1 - N_{\mathrm{KT}}}\right)\frac{\partial N_{\mathrm{KT}}}{\partial t} = K_{\mathrm{KT}}(x_c - x) = A_x + \left(\frac{\partial x}{\partial t}\right)_{\mathrm{sc}}, \tag{11}$$

in which the coefficient K_{KT} is greater than zero for active clouds (i.e., $\partial N_{\mathrm{KT}}/\partial t > 0$). It is worth noting that (11) is equivalent to a "symmetric" formulation of the Kuo scheme (see Bougeault 1985b), in which the total tendencies for both temperature and humidity are simply represented as a relaxation toward a single cloud profile (i.e., x_c) and are split into contributions from cumulus activity and all other processes (A_x). Because ABL moistening due to surface fluxes is in quasi equilibrium with drying by condensation and vertical transport from shallow cumulus activity, we assume that the A_q term is directly related to the boundary layer vertical diffusion, that is, $A_q \approx D_q$ where D_q is the vertical diffusion tendency of specific humidity. In a manner consistent with the nonsteady cumulus cloud model of Kuo (1965), the closure assumptions of the Kuo Transient scheme are completed by neglecting the A_T term, which leads to the following shallow convective tendencies for temperature and specific humidity:

$$\left(\frac{\partial T}{\partial t}\right)_{\mathrm{sc}} = K_{\mathrm{KT}}(T_c - T) \quad \text{and}$$

$$\left(\frac{\partial q_v}{\partial t}\right)_{\mathrm{sc}} = K_{\mathrm{KT}}(q_{vc} - q_v) - D_q. \tag{12}$$

The K_{KT} coefficient is calculated using the energy conservation principle:

$$\int\left(\frac{\partial h}{\partial t}\right)_{\mathrm{sc}} = c_p\int\left(\frac{\partial T}{\partial t}\right)_{\mathrm{sc}} + L\int\left(\frac{\partial q_v}{\partial t}\right)_{\mathrm{sc}} = 0, \tag{13}$$

in which $h = c_pT + Lq_v$ is the enthalpy, and the vertical integrals are done over the cloudy portion of each model column. Developing (13) yields

$$K_{\mathrm{KT}} = \frac{L\int D_q}{c_p\int(T_c - T) + L\int(q_{vc} - q_v)}. \tag{14}$$

The in-cloud values of temperature and specific humidity (T_c and q_{vc}), as well as the cloud water content, are obtained from a simple plume model (Louis 1984). The cloud fraction, N_{KT}, is derived from (11):

$$\frac{\partial N_{\mathrm{KT}}}{\partial t} = K_{\mathrm{KT}}(1 - N_{\mathrm{KT}}), \tag{15}$$

which can be solved in an implicit manner for N_{KT}:

$$N_{\mathrm{KT}} = \frac{K_{\mathrm{KT}}\tau_{\mathrm{sc}}}{1 + K_{\mathrm{KT}}\tau_{\mathrm{sc}}}, \tag{16}$$

where τ_{sc} is a shallow cumulus time scale of 15 min.

Although the Kuo Transient scheme seems quite different from mass-flux designs that are often used to represent cumulus clouds (e.g., von Salzen and McFarlane 2002; Deng et al. 2003), its closure is physically based and the original manner to determine K_{KT}, which is in essence a detrainment coefficient. Representation of precipitation and of vertical transport of momentum associated with overshooting Cu clouds are currently being included in Kuo Transient, but are not part of the present study.

3. Case study

The meteorological situation that occurred over the Pacific Ocean between 6 and 11 February 2003 is used here to examine the behavior of the cloud schemes described in the previous section. During these 5 days, two large-scale weather systems moved eastward toward North America but were either diverted or dissipated as they encountered an intense and stationary high pressure regime in the northeastern quadrant of the Pacific Ocean.

This blocking situation is clearly seen in Fig. 1, which shows the CMC analyses of sea level pressure and 6-hourly precipitation. [These precipitation "analyses" are directly obtained from the 6-h trial forecasts performed in the operational three-dimensional variational data assimilation (3DVAR) and are only used here as a crude approximation of observed precipitation.] In these analyses, the first large-scale baroclinic system (indicated by the letter "A," with central sea

Unauthenticated | Downloaded 08/13/24 05:34 PM UTC

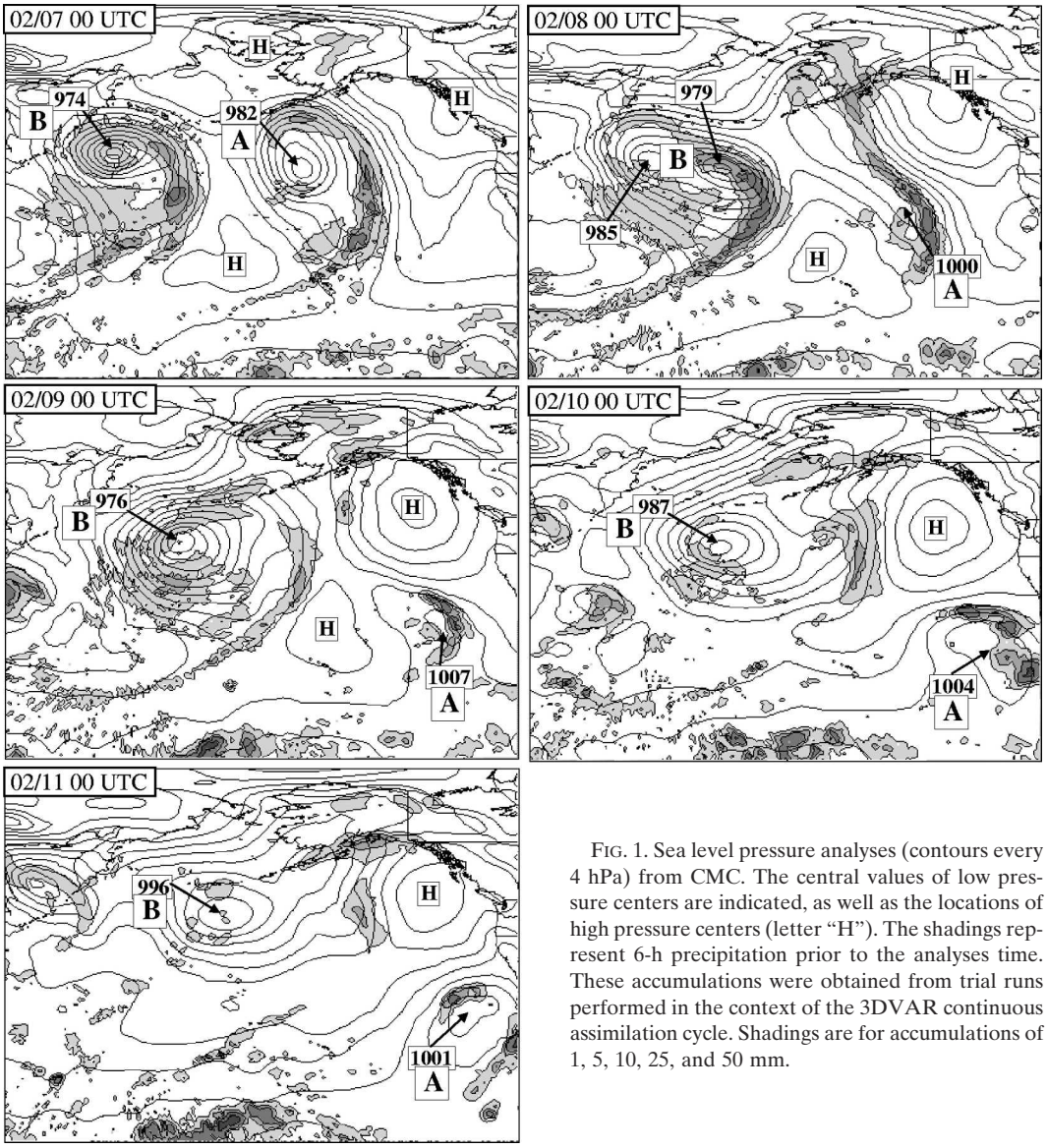

FIG. 1. Sea level pressure analyses (contours every 4 hPa) from CMC. The central values of low pressure centers are indicated, as well as the locations of high pressure centers (letter "H"). The shadings represent 6-h precipitation prior to the analyses time. These accumulations were obtained from trial runs performed in the context of the 3DVAR continuous assimilation cycle. Shadings are for accumulations of 1, 5, 10, 25, and 50 mm.

level pressure of 982 hPa at 0000 UTC 7 February) rapidly advanced eastward and eventually split in two parts as it impinged on the anticyclonic circulation just west of the North American continent. The northern remnant of the large-scale system was later captured by the cyclonic circulation associated with the second large-scale depression. The southern portion of the system was more active, produced more precipitation, and reintensified before hitting the southwestern coast of the United States with several floods (particularly in California). On 6–7 February, the second baroclinic low pressure system (indicated by the letter "B") advanced slowly eastward, before stopping and remaining near the center of the Pacific Ocean for the next few days, with a central sea level pressure of 976 hPa at 0000 UTC 9 February. The depression lost its intensity and filled after this time. At this stage, the main precipitation band separated from the large-scale low pressure center, which became occluded. This precipitation band then dissipated as it reached the stable high pressure region west of Canada.

The visible and infrared images from the Geostationary Operational Environmental Satellites (GOES) reveal the diversity of clouds that were observed over the Pacific Ocean during this period (see Fig. 2). The main cloud band of system B, which is easily recognized in these satellite images, was preceded, as well as followed, by a wide variety of clouds. As the precipitation band evolved eastward and slightly turned northward due to the cyclonic circulation of the occluded low pres-

Unauthenticated | Downloaded 08/13/24 05:34 PM UTC

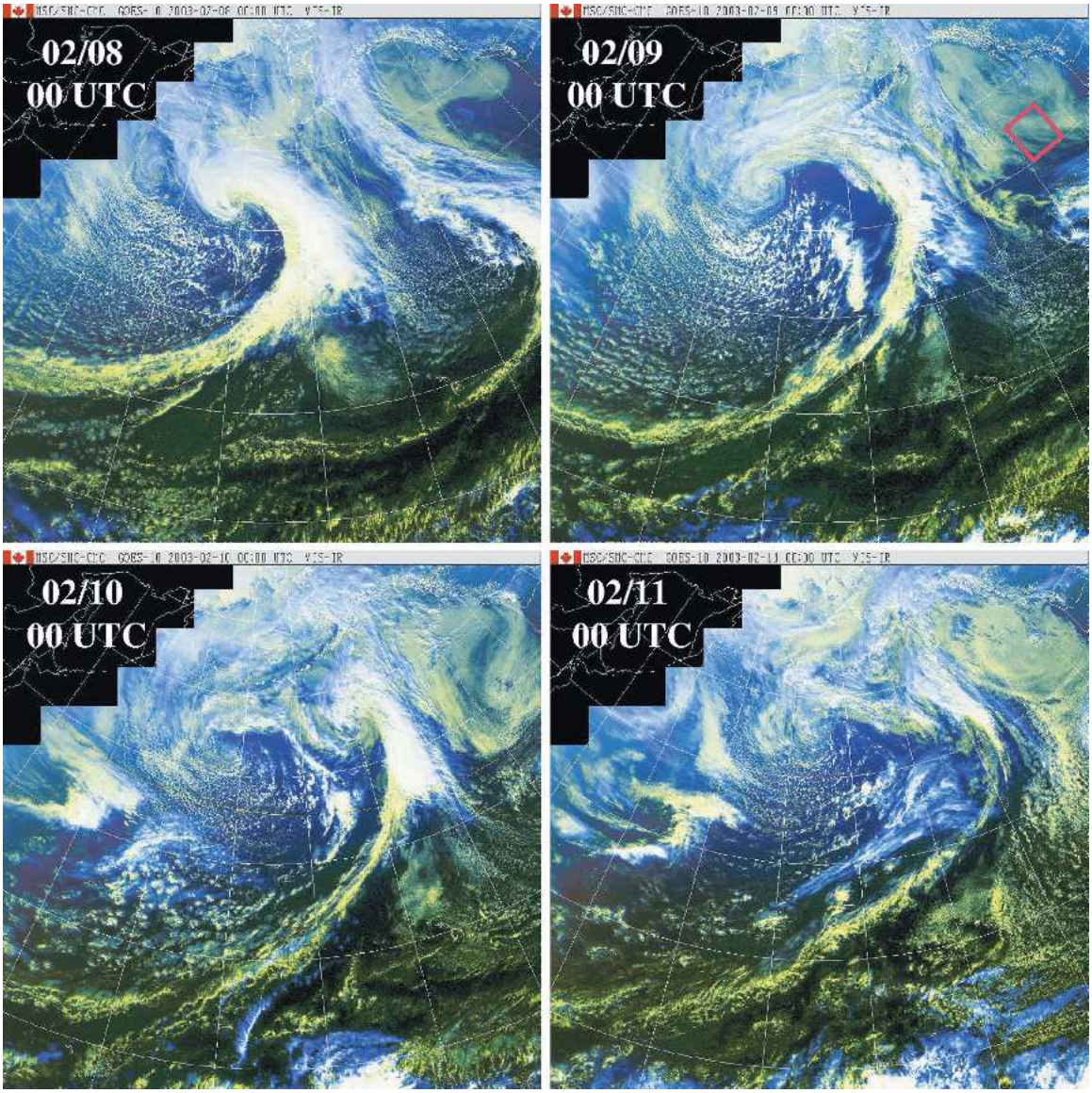

FIG. 2. GOES visible satellite images, with colors indicating cloud-top heights as obtained from infrared information (white color for high-level cloud tops, and yellow color for low-level cloud tops). The box in the upper-right panel indicates the position of the satellite image shown in Fig. 9. Note that the projection used for these images is not the same as the projection used for the maps shown in Fig. 1.

sure center, more intense convection developed in the cold air at the rear of the system (see satellite image for 0000 UTC 9 February). This convective activity later organized in several bands of increasing depth and intensity, from the Cu clouds near the depression's center to the deep convection right behind the main cloud band, as shown by the image for 0000 UTC 10 February. At this time, convective activity within the main cloud band remained intense and well organized, even though its separation from the system's low pressure center increased. The precipitation band finally entered its dissipation phase as it collided with a wide region of Sc clouds located within the high pressure system just west of British Columbia's coast. At the end of the observation period (i.e., 0000 UTC 11 February), the Pacific Ocean was almost entirely covered by clouds, whose type greatly differed depending on their location with respect to the principal cloud band, mainly dissipated at this time. Behind it, shallow-to-intermediate convective activity still occurred, while ahead of it a smooth transition from Sc clouds near Canada's west coast to Cu clouds in the subtropics was observed.

In the rest of this paper, we assess the ability of the GEM atmospheric modeling system to represent this

Unauthenticated | Downloaded 08/13/24 05:34 PM UTC

wide variety of clouds, we examine the role and importance of each cloud scheme (i.e., MoisTKE, Kuo Transient, Kain–Fritsch, and Sundqvist schemes), and we discuss the impact that Sc and Cu clouds may have had on the evolution of the second large-scale weather system (i.e., system B).

4. Results

a. Model representation of clouds

A 5-day control forecast (experiment CTRL) of this Pacific case was done with the uniform-resolution GEM. The configuration used for the numerical experiment is given in Table 2 and includes both the MoisTKE and Kuo Transient schemes. The model was initialized at 0000 UTC 6 February 2003 from CMC's global operational analysis.

A comparison between Figs. 1 and 3 reveal how well GEM was able to predict the sea level pressure fields associated with the two large-scale weather systems. It is worth noting, for instance, how close the forecast and analyzed pressure fields remain throughout the 5-day runs. Both the location and central values of the pressure systems are well represented.

The 6-h precipitation fields in Figs. 1 and 3 are also in good agreement, but this does not tell much about the quality of GEM's precipitation forecast for this particular case because, as explained earlier, precipitation fields in Fig. 1 are not real "analyses" (i.e., no observations of precipitation were used) but rather model outputs from 6-h trial runs performed within the three-dimensional variational assimilation cycle. Nevertheless, the precipitation associated with weather system B seems to be reasonably well predicted, as it exhibits the same features already noted from the satellite imagery shown in Fig. 2: a well-organized precipitation band in the early stages of the forecast (0000 UTC 8 February), a secondary band followed by weak and disorganized events during the occlusion phase (see 0000 UTC 9 February), and scattered and disorganized precipitation events in the late stages of the forecast (0000 UTC 11 February).

Clouds, another feature difficult to evaluate, are shown in Fig. 4. Even though model-produced cloud water content and cloud coverage fraction do not compare easily with finescale details from satellite images, examination of Figs. 2 and 4 reveals that GEM was able, at least in a qualitative manner, to represent correctly the main features of the two large-scale weather systems. For instance, Fig. 4 shows that GEM could produce the two main cloud bands as well as the extensive cloudy areas behind each band. Of particular interest is the transition in system B, at 0000 UTC 9 February, from the main cloud band with large cloud water contents, to (going westward) a relatively wide region clear of clouds, to a smaller secondary band with significant cloud water, to finally more disorganized clouds at the rear of the system. These mesoscale cloud structures later dissipated and transformed into, after 5 days of integration, spiraling cloud bands covering most of the Pacific Ocean. One should finally note the oceanic clouds extending from Alaska to the Tropics, between the North American coast and the two weather systems, which are also observed in Fig. 2.

TABLE 2. Configuration of numerical experiments.

Experiment	ABL scheme	Shallow convection
CTRL	MoisTKE	Kuo Transient
NOKT	MoisTKE	None
NOMTKE	TKE "dry"	Kuo Transient
NOSHAL	TKE "dry"	None

A first step toward a more quantitative evaluation of the clouds produced by GEM is offered in Fig. 5, in which the vertically integrated liquid cloud water obtained from Special Sensor Microwave Imager (SSM/I) instruments is compared with model results. This figure shows again the general features of the second large-scale weather system (cf. Figs. 2 and 5), but it also reveals some weaknesses of the clouds produced by the model. One of these problems is related to the propagation speed of the main cloud band, which seems to be too rapid (this could be explained, at least partly, by the difference in the validity times of the observations and model outputs). Of greater importance are the differences that are found in the cumulus regime in the rear portion of the large-scale system. A first difference, not unexpected, is the smaller horizontal variability of model-produced cloud liquid water content compared with observations. With grid sizes on the order of 35 km at these latitudes, the model is not able to resolve the small-scale features of cumulus activity. Another difference, more relevant in our opinion, is related to the relatively large values of vertically integrated liquid water predicted in this region (greater than 0.10 kg m^{-2}, compared with observations between 0.01 and 0.10 kg m^{-2}). The reasons why such a disparity exists between model results and observations are unknown at this point; rigorous and exact representation of cloud water *amounts* are beyond the scope of the current investigation.

As described above, several schemes are responsible for the clouds produced by GEM. Figure 6 indicates where each cloud scheme is mostly responsible for the cloud coverage. (The dominant cloud type was obtained from the vertically integrated grid-scale cloud

Unauthenticated | Downloaded 08/13/24 05:34 PM UTC

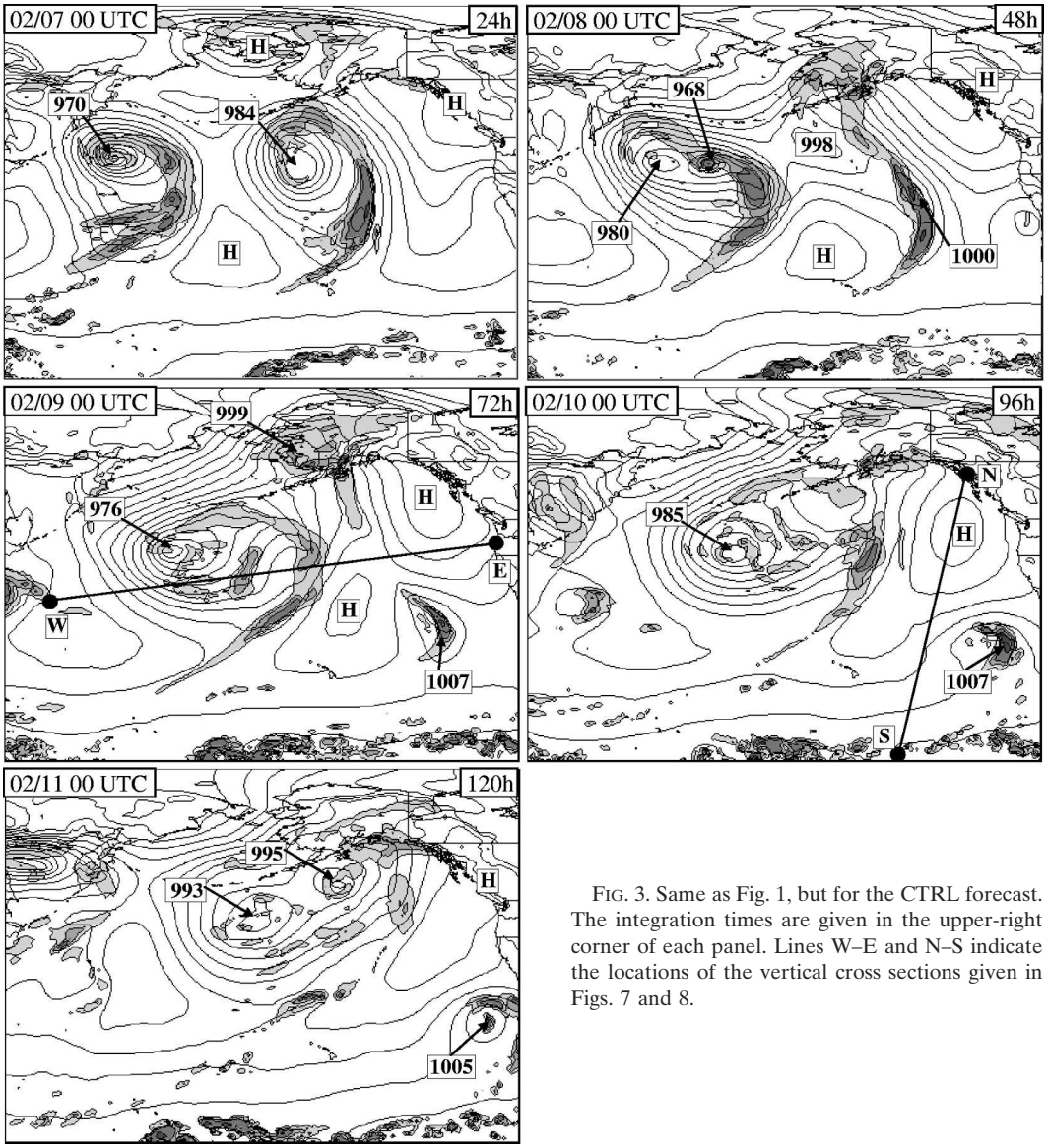

FIG. 3. Same as Fig. 1, but for the CTRL forecast. The integration times are given in the upper-right corner of each panel. Lines W–E and N–S indicate the locations of the vertical cross sections given in Figs. 7 and 8.

water content from each of the cloud scheme. Where deep convection occurred, the Kain–Fritsch scheme was automatically assumed to be the dominant cloud scheme.)

One first notes from Fig. 6 that the Kain–Fritsch scheme for deep convection is not very active at 0000 UTC 9 February (72-h integration). This scheme only produces clouds and precipitation over small regions within the main precipitation band of system A and in the rear portion of system B. Interestingly, the second band in this last system exhibits more deep convective activity than the leading precipitation band. The Kain–Fritsch scheme was already shown to behave in this manner for strongly forced weather systems, in which most of the clouds and precipitation occur on the grid scale (see Bélair et al. 2000). For the leading precipitation band of system B, the atmospheric forcing (or vertical motion) associated with baroclinic instability is sufficient to produce saturation at the model grid scale, so that the nonconvective condensation scheme (i.e., Sundqvist scheme) produces most of the clouds and precipitation.

As could be expected from the satellite images shown in Fig. 2, clouds in the rear portion of the two large-scale systems are essentially produced by the Kuo Transient cumulus scheme. In both satellite observations and model results, these cumulus clouds spread over large areas, especially for system B. The cloud patches near British Columbia's coast, on the other hand, are chiefly the results of the MoisTKE vertical diffusion

Unauthenticated | Downloaded 08/13/24 05:34 PM UTC

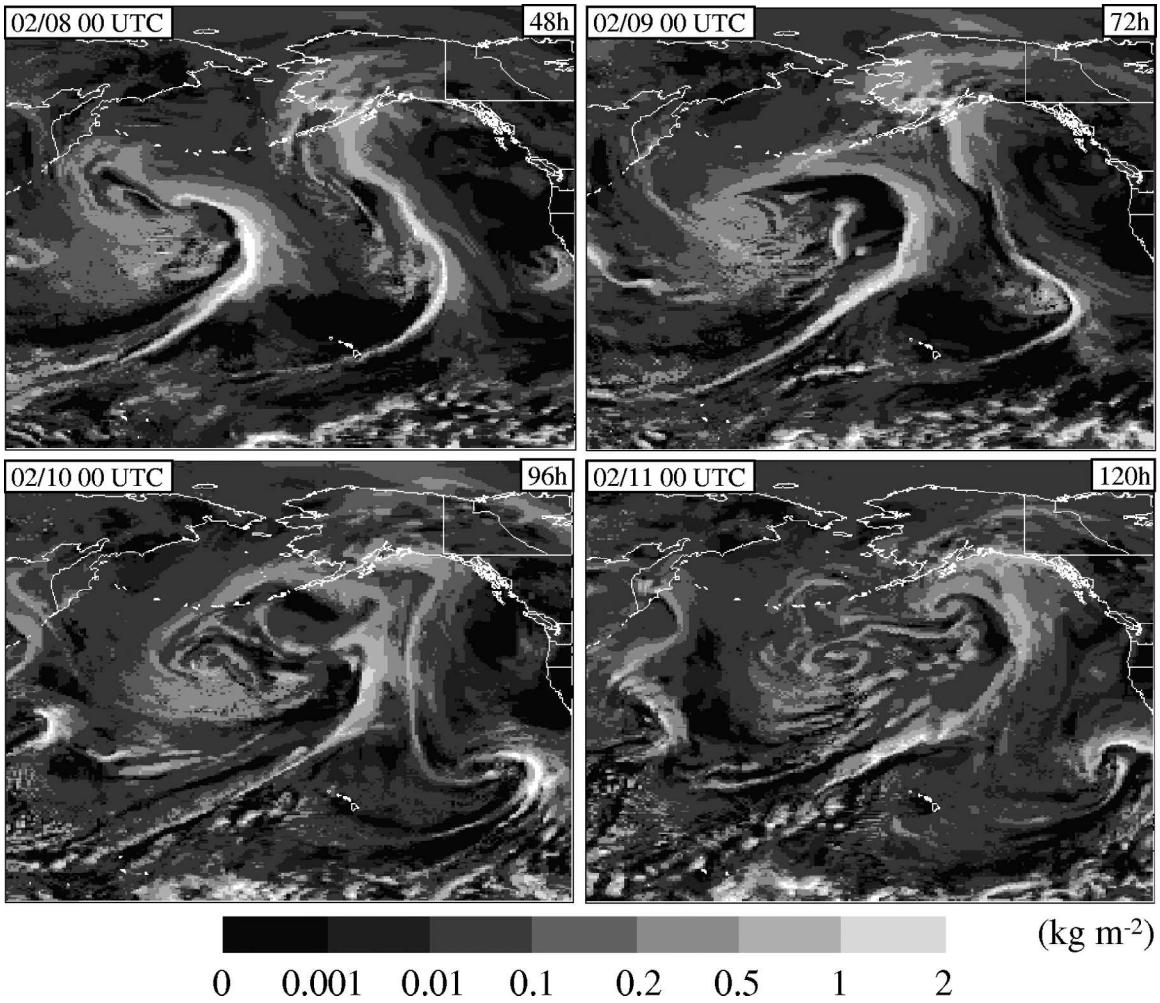

FIG. 4. Vertically integrated total cloud water (in kg m^{-2}, or mm) from the CTRL forecast. The total cloud water includes contributions from all the cloud schemes, i.e., MoisTKE, Kuo Transient, Kain–Fritsch, and Sundqvist schemes.

scheme, and are thus represented as boundary layer clouds in GEM. This seems appropriate since Fig. 2 indicates that these clouds occur at low levels.

The vertical structures in Fig. 7 show that the main cloud band of system B extends to levels higher than 10 km and is dynamically forced by upward motion of sufficient intensity to produce grid-scale condensation. In contrast, the second band of this system experiences weaker vertical motion and does not extend as high (i.e., 8 km). Cloud water contents are also less for this band, compared with the leading cloud band. In the rear portion of the system, cumulus convection produced by the Kuo Transient scheme is capped by large-scale subsidence. As subsidence decreases eastward toward the main precipitation band, the depth of the Kuo Transient cumulus clouds increases from less than 2 km near the western edge of the system to about 4 km just behind the second cloud band. For the same reasons, the Kain–Fritsch deep convection scheme is also more active in this region and may be responsible for at least part of the upper-level anvil of nonconvective clouds just behind the second precipitation band. Figure 7 also shows that the thin layer of boundary layer clouds, produced by the MoisTKE scheme near the North American West Coast, occurs in a weak northerly circulation. The vertical motion, or dynamical forcing, is weak in this region.

Cross sections of the same type are given in Fig. 8, but for the 96-h forecast (valid at 0000 UTC 10 February) along a north–south line ahead of the two large-scale systems. Over this region, GEM produced a shallow layer of clouds with height and depth increasing toward the Tropics. In the midlatitudes, the thin clouds mostly develop in the ABL and are associated with the MoisTKE vertical diffusion scheme. In the subtropical region, where sources of heat and moisture from the

Unauthenticated | Downloaded 08/13/24 05:34 PM UTC

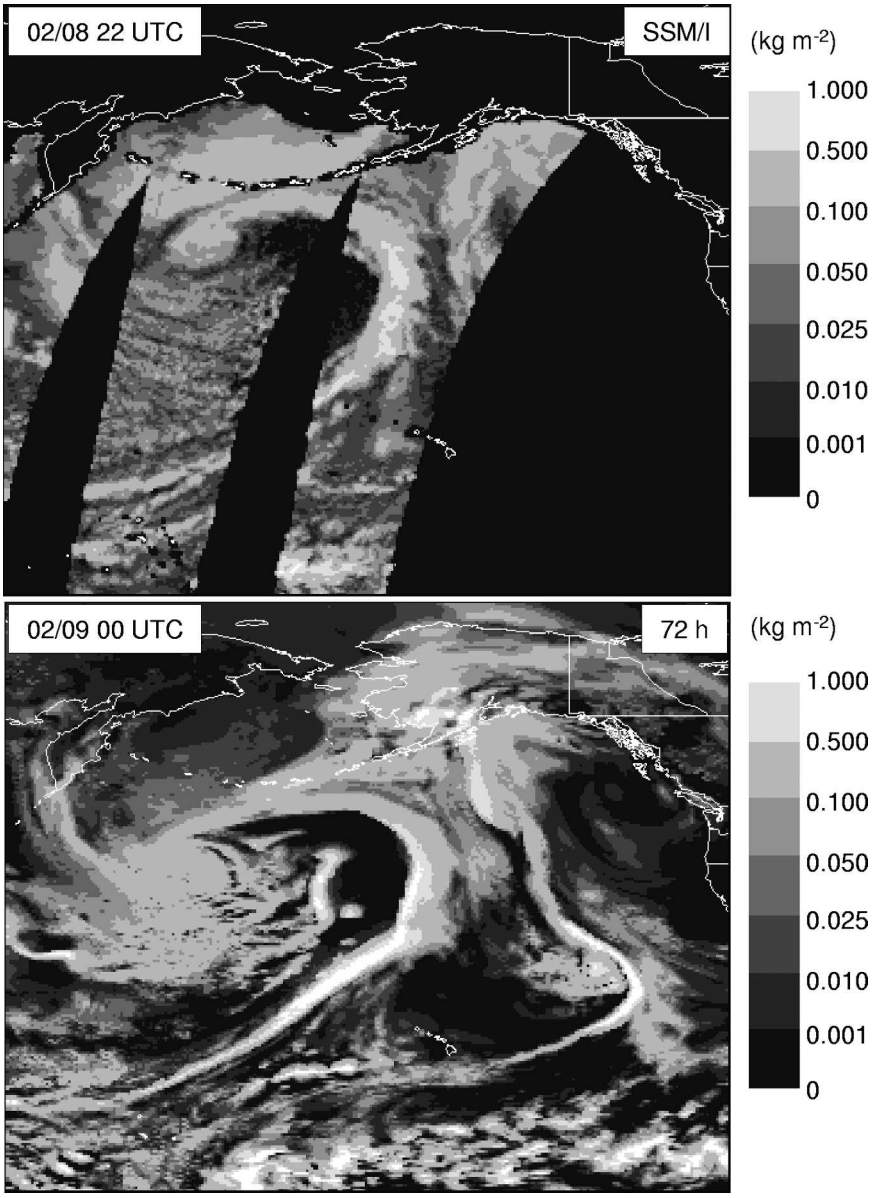

FIG. 5. Vertically integrated liquid cloud water (in kg m^{-2}, or mm) from the SSM/I and the CTRL (72 h) forecast. As in Fig. 4, the cloud water includes contributions from all the cloud schemes. It should be noted that the measurements and model outputs are not valid at the same time (SSM/I data were collected between 2000 UTC 8 Feb and 0000 UTC 9 Feb, and model results are valid at 0000 UTC 9 Feb). Also, the contours are not identical to those of Fig. 4.

ocean surface are greater, the low-level clouds become deeper, more scattered, and are mostly produced by the Kuo Transient cumulus scheme. In the Tropics, finally, the weaker subsidence allowed the Kain–Fritsch scheme to produce some deep convection.

Comparison with the satellite images in Fig. 2 indicates that this transition, from thin ABL clouds, to scattered overshooting Cu clouds, to deep convection in the Tropics, appears to be qualitatively correct. It seems, however, that the cloud fraction predicted for the midlatitude low-level clouds is significantly underpredicted by the MoisTKE scheme. Figure 2, as well as the high-resolution satellite imagery given in Fig. 9, shows the presence of large sheets of stratocumulus clouds over this region, with cloud fractions of at least 50%, which is significantly larger than the cloud coverage produced

Unauthenticated | Downloaded 08/13/24 05:34 PM UTC

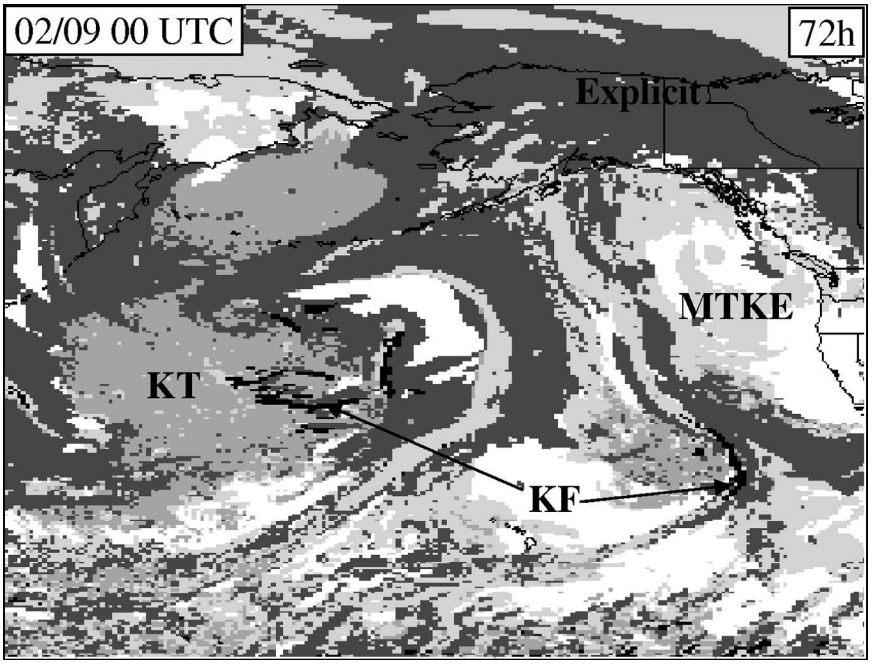

FIG. 6. Map of dominant cloud type from the 72-h CTRL forecast, valid at 0000 UTC 9 Feb 2003. The dominant cloud type is determined from the vertically integrated cloud water produced by each cloud scheme, i.e., MoisTKE (MTKE), Kuo Transient (KT), Kain–Fritsch (KF), and Sundqvist (grid scale) schemes.

by MoisTKE (approximately 10% over the same region).

b. Role and importance of MoisTKE and Kuo Transient cloud schemes

The results presented above clearly establish that GEM, with its four-scheme cloud package (CTRL run), is able to represent in a qualitatively correct manner the wide variety of clouds observed during 6–11 February over the Pacific Ocean. To examine the role and importance of the clouds produced by the MoisTKE and Kuo Transient schemes, two additional forecasts are discussed in this section: experiment NOKT, identical to the CTRL run except that the Kuo Transient scheme is turned off, and experiment NOSHAL, identical to NOKT except that MoisTKE is not used; that is, a "dry" vertical diffusion scheme is active instead, with diffusion performed on the equivalent potential temperature and specific humidity, with no effect of clouds. The configurations used for these sensitivity experiments are summarized in Table 2.

Results from these two experiments point out the rear portion of system B as the region where most of the sensitivity associated with the two cloud schemes resides. Therefore, the argumentation presented in the rest of this section is based on profiles of cloud and thermodynamic characteristics averaged over region A of the cross sections shown in Fig. 7.

In Fig. 10, the mean cloud water content from the Sundqvist nonconvective cloud scheme (left), and the total cloud coverage fraction obtained from random overlap of all the cloud schemes' fractions (right), are given for the three numerical experiments. These results show that if no parameterization of Sc and Cu clouds is used in GEM (experiment NOSHAL), the model produces a low-level layer of nonconvective clouds in the rear portion of system B. The mean total cloud fraction over this area is greater than 70%, and the mean grid-scale cloud water content is as large as 0.20 g kg^{-1}. Obviously, these cloud characteristics are not consistent with the Cu activity pictured in the satellite imagery in Fig. 2. Not surprisingly, GEM is not able to generate the subgrid-scale clouds observed over this region without MoisTKE and/or Kuo Transient. In NOSHAL, the only subgrid-scale cloud scheme remaining is the Kain–Fritsch scheme for deep convection. Although the activity of this scheme is increased in NOSHAL compared with the control run (as discussed in the next subsection), the Kain–Fritsch scheme is not appropriate for the shallow convective clouds discussed here and is not able to prevent the generation of nonconvective clouds.

Comparison of experiments NOSHAL and NOKT in

Unauthenticated | Downloaded 08/13/24 05:34 PM UTC

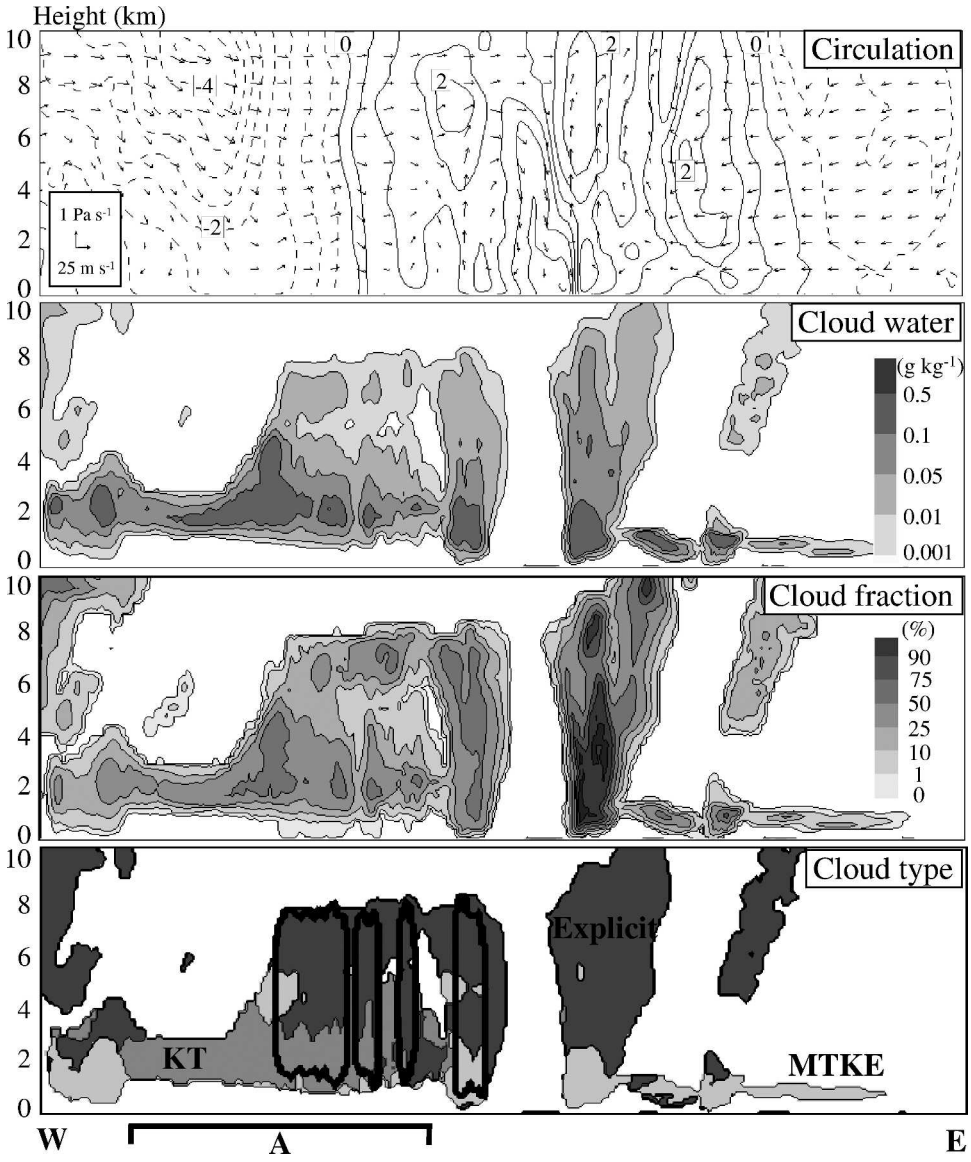

FIG. 7. Vertical cross sections along line W–E in Fig. 3 from the 72-h CTRL forecast valid at 0000 UTC 9 Feb 2003. (top) The along- and across-line circulations, with arrows and contours (every 0.5 m s^{-1}) respectively. (second from top) The total cloud water (g kg^{-1}), (third from top) the total cloud fraction (%), and (bottom) the dominant cloud type. The along-line circulations are relative to the main precipitation band motion (i.e., a mean propagation speed of 8 m s^{-1} was subtracted from the east–west wind component). The cloud type was determined as in Fig. 6. All the above meteorological quantities were averaged in the cross-line direction, and these panels thus in fact represent mean vertical cross sections along a 500-km band following line W–E.

Fig. 10 indicates that MoisTKE mainly contributes in lifting (by 600–800 m) this low-level cloud layer, without significantly reducing the associated nonconvective cloud water content or total cloud fraction. This is consistent with the mean tendencies shown in Fig. 11, which suggest that the main impact of MoisTKE, compared with the "dry" vertical diffusion scheme, is to increase the exchanges between the ABL and free atmosphere. The main effect of this increased vertical diffusion is to produce a deeper, warmer, and drier ABL, as well as a cooler, more humid free atmosphere (Fig. 12).

In contrast, the Kuo Transient cumulus scheme causes little change to the average height of the cloud layer, but succeeds in considerably decreasing the nonconvective contribution to these clouds (cf. experi-

Unauthenticated | Downloaded 08/13/24 05:34 PM UTC

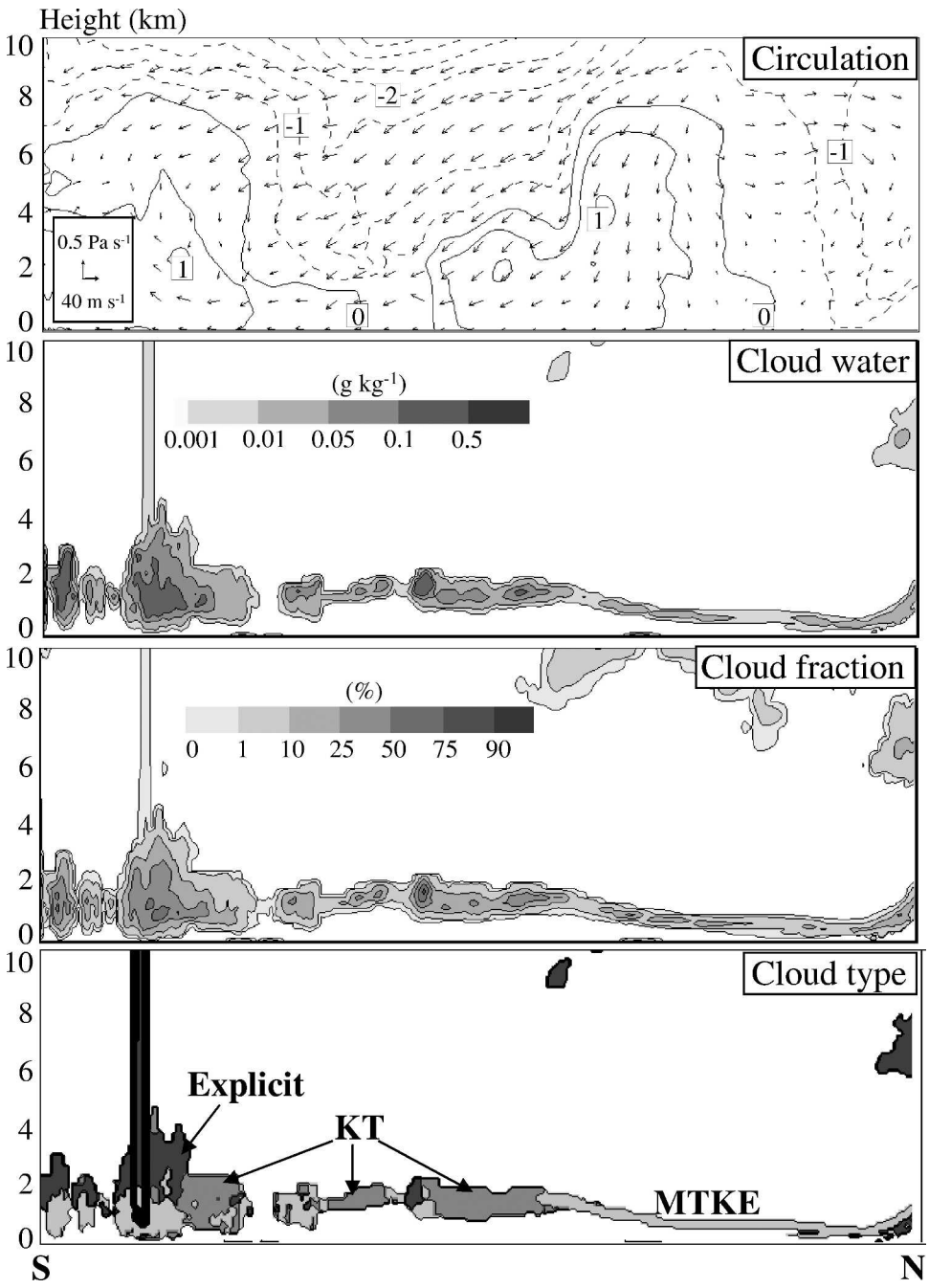

FIG. 8. Same as Fig. 7 but for the line N–S in Fig. 3 and for the 96-h CTRL forecast, valid at 0000 UTC 10 Feb 2003.

ments CTRL and NOKT in Fig. 10). With Kuo Transient, the total cloud fraction is about 40% in the rear portion of system B (compared with 60% in experiment NOKT), and cloud water content from the nonconvective cloud scheme is reduced by almost an order of magnitude (from 0.17 g kg^{-1} in experiment NOKT to 0.02 g kg^{-1} in experiment CTRL).

As shown in Fig. 11, the role of the Kuo Transient scheme is mainly to warm and dry the cloud layer, a process more similar to vertical stabilization normally expected of convective schemes (see Kain and Fritsch 1990), but quite different from the diffusive response of MoisTKE. It should be noted from Fig. 11 that because of its simplicity, Kuo Transient does not represent the

Unauthenticated | Downloaded 08/13/24 05:34 PM UTC

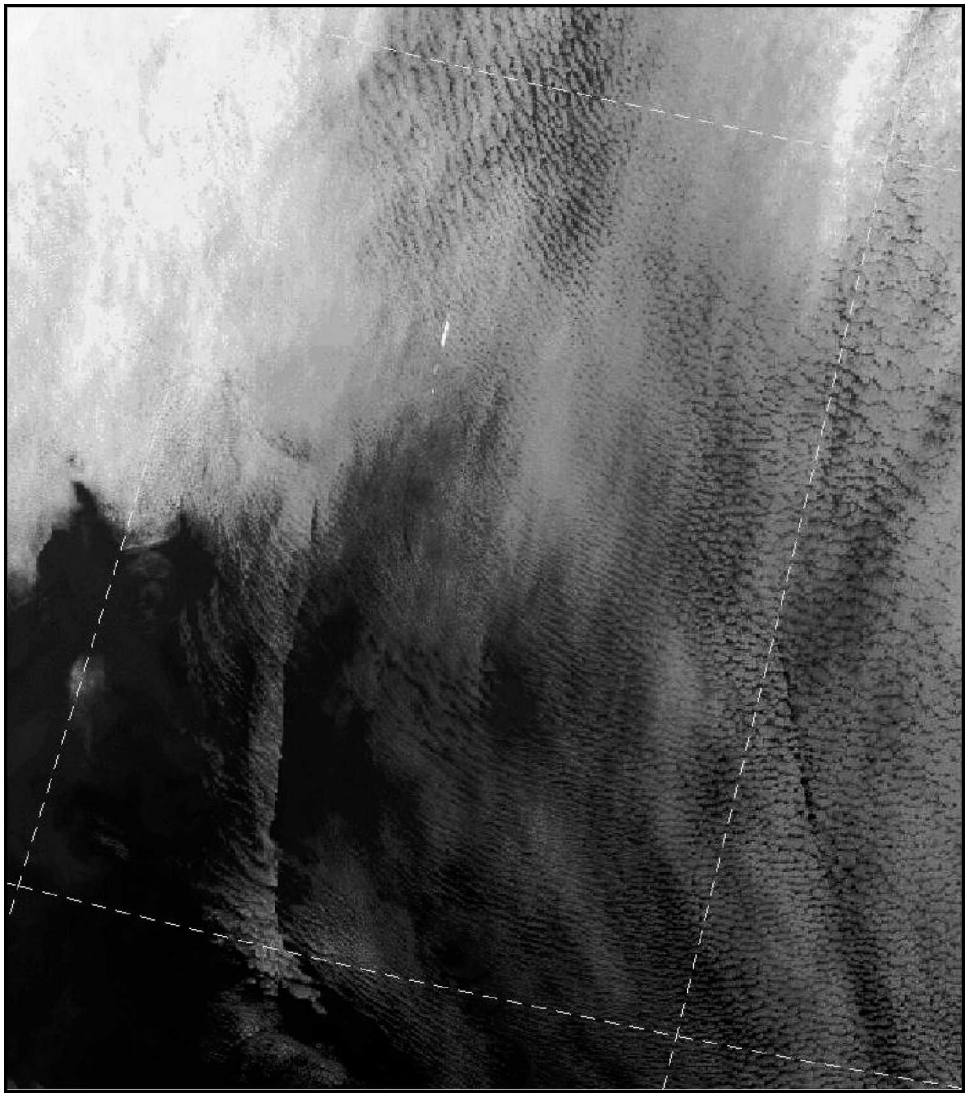

FIG. 9. Satellite image obtained from an Advanced Very High Resolution Radiometer (AVHRR), valid at 0700 UTC 9 Feb 2003. The location of this image is indicated in Fig. 2.

cooling from evaporation and sublimation of precipitation that could occur below cloud base.

Surprisingly, the largest changes in the mean vertical thermodynamic profiles resulting from Kuo Transient's convective stabilization is found in the ABL, which becomes much warmer and drier when this scheme is used, even though its largest tendencies are found in the free atmosphere just above the ABL (cf. Figs. 11 and 12). The reason for this large impact of Kuo Transient on the ABL's temperature and humidity could be related to the turbulent entrainment at the top of the ABL, which is enhanced by MoisTKE, and which could explain how heating and drying caused by shallow and overshooting convection (in the free atmosphere) are in fact transferred to the ABL.

Other sensitivity experiments, whose results are not shown, seem to confirm this hypothesis, since they reveal that Kuo Transient has less influence on the ABL's structures when a "dry" vertical diffusion scheme is used instead of MoisTKE. In this case, cumulus activity from Kuo Transient is reduced because of the smaller accession term for humidity [D_q in (12)], while vertical diffusion is less because the effect of clouds is not considered in the turbulence scheme (see Fig. 11). This interaction between MoisTKE and Kuo Transient has the overall effect of increasing surface evaporation (and decreasing sensible heat fluxes), thereby providing even more fuel for further generation of low-level clouds. A positive feedback thus seems to exist between the two cloud schemes.

Unauthenticated | Downloaded 08/13/24 05:34 PM UTC

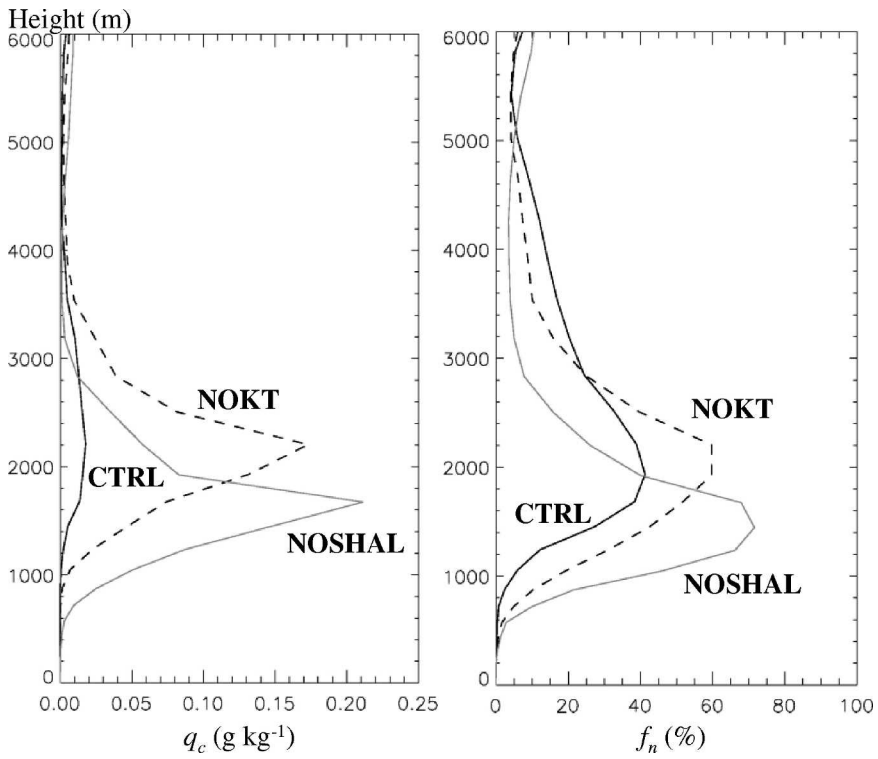

FIG. 10. Mean vertical profiles of cloud water from the (left) nonconvective condensation scheme and of (right) total cloud fraction for the 72-h CTRL, NOKT, and NOSHAL forecasts valid at 0000 UTC 9 Feb 2003. The profiles are averaged over the rear region of the large-scale weather system (see region A in Fig. 7).

The combined effect of MoisTKE and Kuo Transient (see thick full lines in Fig. 11) is to warm a relatively deep portion of the troposphere, that is, up to about 5 km, and slightly cool above this level. For humidity, the total tendencies are limited to the lower troposphere and essentially represent an increase in vertical transport near the top of the ABL. Maxima for drying and moistening occur around 1800 and 2800 m, respectively. This asymmetry between the temperature and humidity total tendencies is related to the larger warming by Kuo Transient (compared with MoisTKE) above the ABL, and the larger drying by MoisTKE (compared with Kuo Transient) near the top of the ABL. How well these tendencies are representative of the Sc and Cu clouds that really occurred during this case is unknown. Detailed observations and/or large-eddy simulations would be needed to assess this point.

c. *Impact of Sc and Cu clouds on the large-scale weather system*

Because the model configuration used in the current study (see Table 1) has been recently implemented in the short-range regional version of GEM used operationally at CMC, and because this configuration is also on the verge of being proposed for the global medium-range version of GEM, it is important to understand the impact that a better representation of Sc and Cu clouds (with MoisTKE and Kuo Transient) has on the predicted evolution of the large-scale weather systems.

First, comparison of Figs. 3 and 13 does not reveal any outstanding difference in the sea level pressure fields produced in the CTRL and NOSHAL integrations. The structure of the sea level pressure fields, as well as the position of the low pressure centers, are very similar in the two forecasts. The two figures indicate, nevertheless, that the two cloud schemes could exert some control on the intensification of the large-scale depressions. It can be noted, for instance, that the second large-scale depression is a few hectopascals deeper when neither MoisTKE nor Kuo Transient are used. This is especially true in the later stages of the 5-day integrations (e.g., 973 versus 976 hPa at 72 h, 984 versus 985 hPa at 96 h, and 991 versus 993 hPa at 120 h).

Precipitation, however, is more sensitive to the representation of Sc and Cu clouds (cf. Figs. 3 and 13). When MoisTKE and Kuo Transient are omitted, pre-

Unauthenticated | Downloaded 08/13/24 05:34 PM UTC

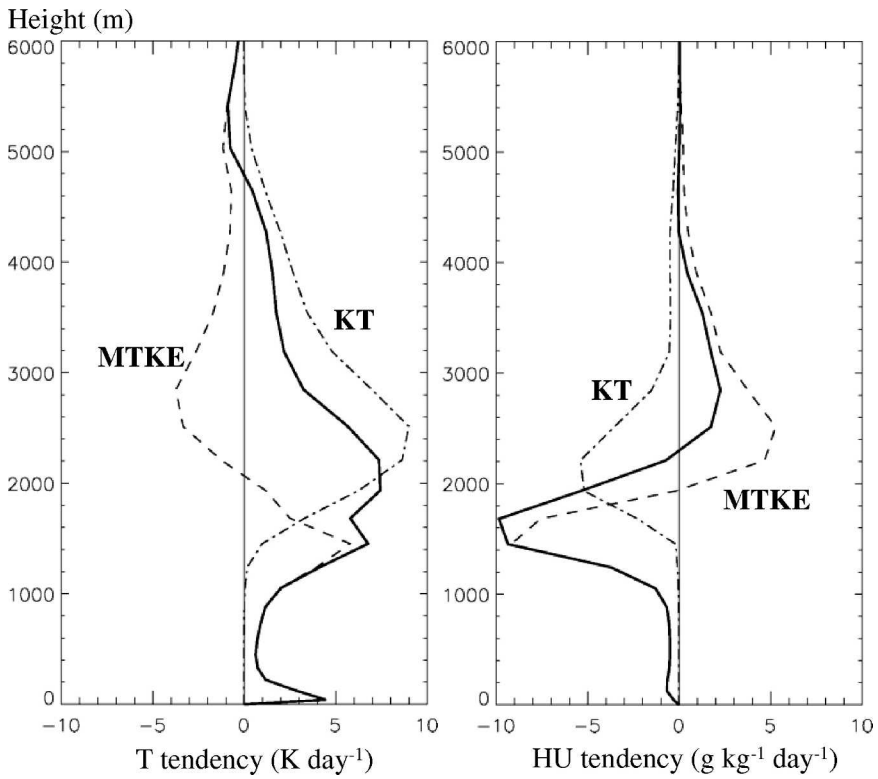

FIG. 11. Mean 24-h tendencies of temperature and humidity from MoisTKE (dash lines) and Kuo Transient (dash–dot lines) for the period preceding 0000 UTC 9 Feb 2003 (i.e., average between 48- and 72-h forecasts). The tendencies are averaged over the same region as in Fig. 10. The impact of MoisTKE (or its overall "tendencies") was obtained by subtracting the vertical diffusion tendencies of the NOMTKE experiment from the CTRL run (the NOMTKE experiment is similar to CTRL, except for the ABC vertical diffusion, which is done using the "dry" TKE version instead of MoisTKE, see Table 2). The thick full lines show the total low-level cloud tendencies resulting from the combination of MoisTKE and Kuo Transient.

cipitation is more widespread and exhibits more small-scale features. In some regions, such as the Tropics and sub-Tropics, precipitation from experiment NOSHAL could even be qualified as "noisy." This type of difference is also found in the rear portion of large-scale system B. Another discrepancy between the two experiments is the forecast, in the later stages of experiment NOSHAL, of a narrow band of precipitation that extends from system B's cold front to the Tropics. Such a band is not produced in the CTRL experiment.

The impact that the two cloud schemes have on precipitation is also shown in Figs. 14 and 15, in the form of east–west cross sections of accumulations. In Fig. 14, one can easily recognize precipitation associated with the main cloud band, the second (convective) band, and the rear portion of the system. The different positions and widths of the two precipitation bands produced in the CTRL, NOKT, and NOSHAL experiments are mainly related to deep convection from the Kain–Fritsch scheme. As described below, deep convection becomes more active when MoisTKE and/or Kuo Transient are not used.

In the rear portion of the system, where both MoisTKE and Kuo Transient were shown to have a strong influence on clouds and on vertical profiles of temperature and humidity, precipitation also appears to be sensitive to the representation of low-level clouds. It seems that the increase in vertical diffusion produced by MoisTKE lead to smoother precipitation in this portion of the system. Also, as nonconvective clouds were shown to be slightly reduced when using this cloud scheme (see Fig. 10), precipitation is also decreased.

The impact of Kuo Transient is even more important, as could be expected from the significant reduction of nonconvective clouds shown in Fig. 10. Indeed, precipitation in the rear portion of the large-scale system becomes almost negligible when using the Kuo Transient cumulus scheme. It should be noted, however, that precipitation associated with the Kuo Transient shallow convective activity is not accounted for in the total pre-

Unauthenticated | Downloaded 08/13/24 05:34 PM UTC

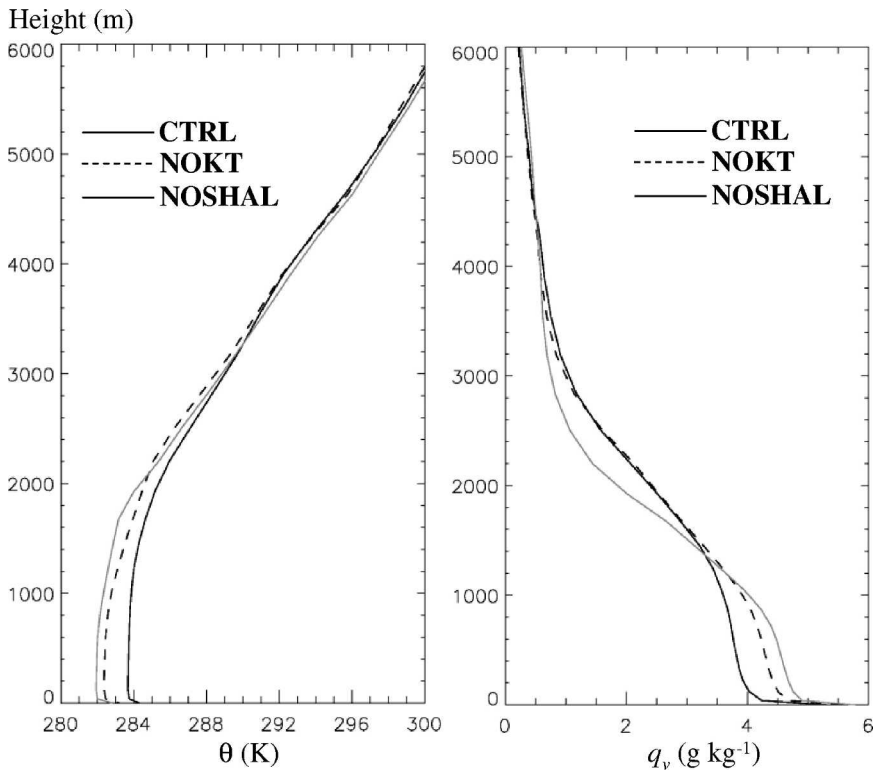

FIG. 12. Comparison of mean vertical profiles of (left) potential temperature θ and (right) specific humidity q_v for the 72-h CTRL, NOKT, and NOSHAL forecasts valid at 0000 UTC 9 Feb 2003. The profiles are averaged over the same region as in Fig. 10.

cipitation shown in Figs. 14 and 15. From the average humidity tendencies given in Fig. 11, this precipitation is estimated to be no more than 2 mm day^{-1} (or 0.5 mm per 6 h), in the rear portion of system B. Because of the fact that a significant portion of this precipitation would evaporate before reaching the surface, its omission does not change the conclusion regarding the decrease of precipitation associated with the use of Kuo Transient.

The same kind of impact is also observed in the 5-day precipitation accumulations shown in Fig. 15. Both cloud schemes contribute to reduce the total precipitation (upper panel). When the Kuo Transient scheme is used, total precipitation is approximately reduced by half in the rear portion of the system (~40 mm in experiments NOKT and NOSHAL versus 20 mm in experiment CTRL). The lower panel of Fig. 15 reveals that both the convective and nonconvective components of the precipitation were affected by the inclusion of MoisTKE and Kuo Transient.

To help understand why convective and nonconvective precipitation is reduced when using MoisTKE or Kuo Transient, equivalent potential temperature (θ_e) profiles are shown in Fig. 16. These profiles provide information on the conditional instability (i.e., when $\partial\theta_e/\partial z<0$) present in the rear portion of the large-scale system. By promoting the upward transport of high-θ_e air from the ABL to the free atmosphere, both MoisTKE and Kuo Transient have the effect of reducing the conditional instability in this portion of the system. This vertical stabilization could explain why deep convection is less active in the CTRL and NOKT experiments (compared with the NOSHAL experiment).

Because of the complexity of the interactions that exist between convective and nonconvective condensation schemes (see Molinari and Dudek 1992; Zhang et al. 1994), it is difficult to determine exactly what is the impact of reducing Kain–Fritsch's precipitation, and more importantly its associated vertical stabilization. Because of a compensation effect, decrease of implicit activity usually results in an increase of nonconvective condensation and precipitation. In the present study, this is obviously not the case, since both convective and nonconvective precipitation is reduced when using the two low-level cloud schemes (particularly Kuo Transient). In the present study, it seems that the ability of the Kuo Transient scheme to virtually eliminate the

Unauthenticated | Downloaded 08/13/24 05:34 PM UTC

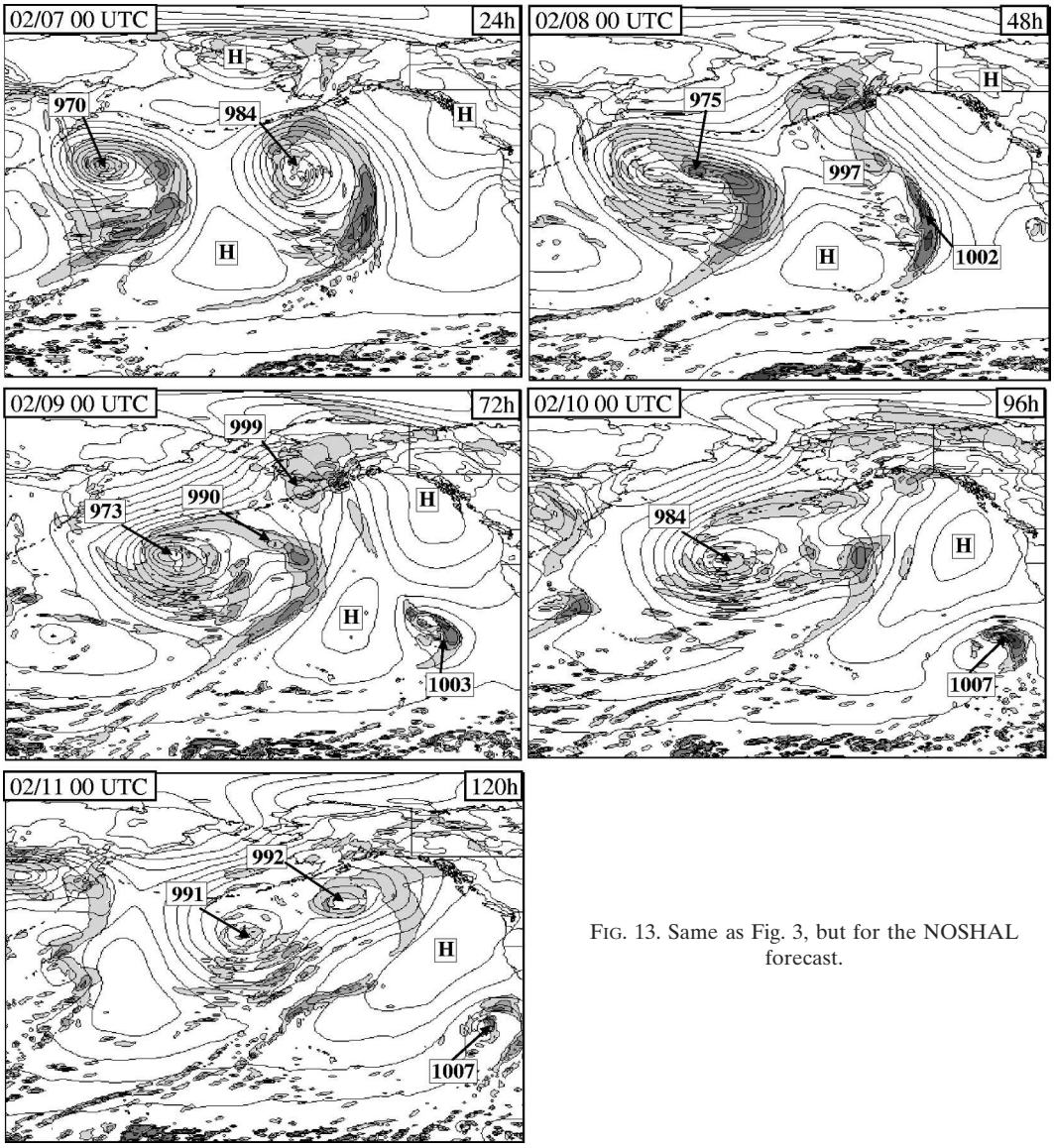

FIG. 13. Same as Fig. 3, but for the NOSHAL forecast.

presence of grid-scale saturation and clouds in the rear portion of the system (see Fig. 10) is the reason why nonconvective precipitation is dramatically reduced when using this scheme, in spite of the decrease of vertical stabilization from the deep convection scheme. Obviously, the additional stabilization provided by the Kuo Transient cumulus scheme more than compensates what is lost by diminishing the role of the Kain–Fritsch implicit scheme.

5. Summary and conclusions

Our main interest in this study was to discuss the role and impact that boundary layer and shallow cumulus

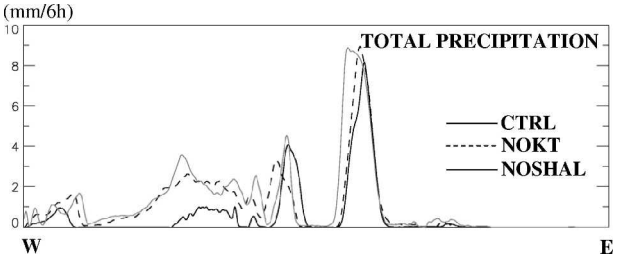

FIG. 14. Comparison of CTRL, NOKT, and NOSHAL forecasts of total precipitation along line W–E in Fig. 3 for the 6-h period ending at 0000 UTC 9 Feb 2003 (i.e., 72-h integration). The precipitation was averaged in the cross-line direction in the same manner as for Figs. 7 and 8.

Unauthenticated | Downloaded 08/13/24 05:34 PM UTC

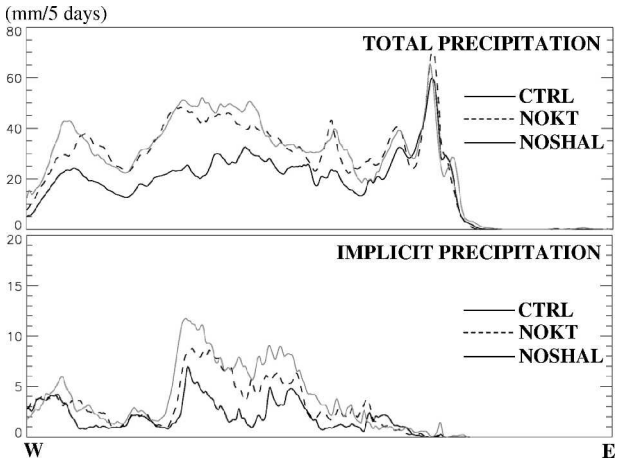

FIG. 15. Comparison of CTRL, NOKT, and NOSHAL forecasts of (top) total and (bottom) implicit (i.e., convective) precipitation along line W–E in Fig. 3 for the entire 120-h forecast (valid at 0000 UTC 11 Feb 2003). The precipitation was averaged in the cross-line direction in the same manner as for Figs. 7 and 8. Note also the different scales for the upper and lower panels.

clouds have on the medium-range forecast of a large-scale weather system that occurred over the Pacific Ocean during February 2003. This was achieved with the GEM atmospheric model, in which a four-scheme condensation package was used: the MoisTKE scheme for boundary layer clouds (stratus, Sc, and small Cu clouds), the Kuo Transient scheme for overshooting Cu clouds, the Kain–Fritsch scheme for deep convection, and the Sundqvist scheme for nonconvective clouds.

The results showed that GEM, with this new cloud package, was able to represent the wide variety of clouds observed during this large-scale meteorological event. In particular, it was found that the Kuo Transient scheme was mostly responsible for the overshooting Cu clouds in the rear portion of the large-scale system, whereas MoisTKE produced the low-level Sc clouds ahead of the system. Several diagnostics calculated for the rear portion of the system revealed that the impact of MoisTKE was mainly to increase the vertical transport (diffusion) associated with the ABL clouds, while Kuo Transient was acting in a manner more consistent with convective stabilization. As a consequence, MoisTKE was not able to remove the low-level shallow cloud layer incorrectly produced on GEM's grid scale by the Sundqvist scheme. Only with Kuo Transient did we see a significant reduction of these nonconvective clouds, in better agreement with satellite observations. This improved representation of Sc and Cu clouds was not found to have a large impact on the overall sea level pressure patterns of the large-scale weather system for a forecast time up to 120 h. It was found, however, that

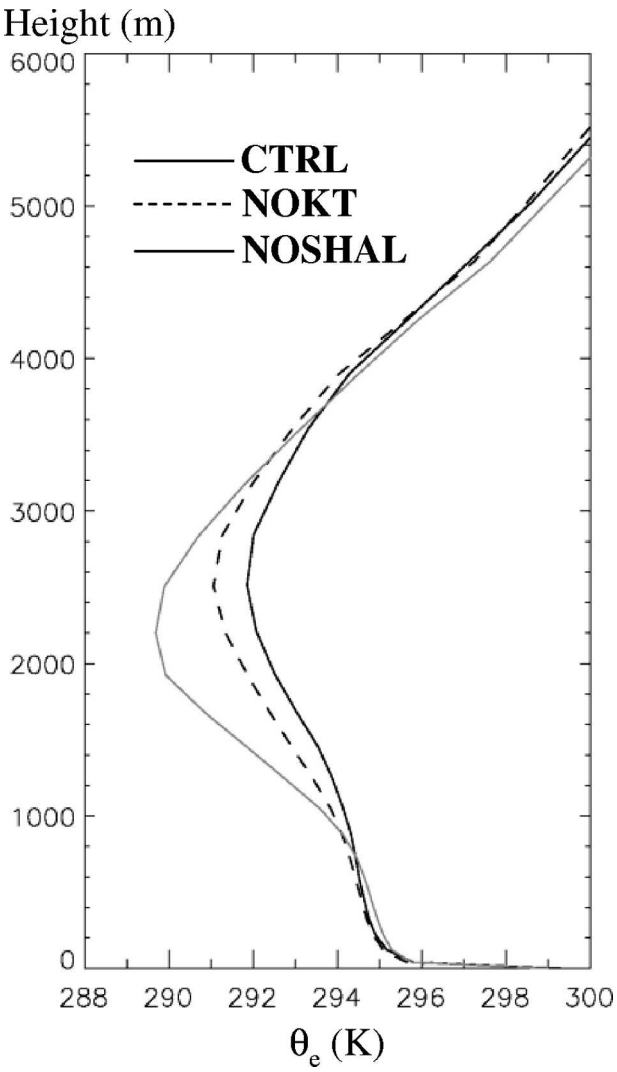

FIG. 16. Same as Fig. 12, but for the equivalent potential temperature θ_e.

precipitation in the rear portion of the system was smoother when MoisTKE was used, and was significantly decreased when the Kuo Transient scheme was switched on.

The generally positive results described in this study were mainly of a qualitative nature, and further comparisons using data from remote sensing, field campaign observations, and high-resolution cloud-resolving models, are currently under way to provide a more quantitative evaluation of the clouds in GEM. These results also encourage us to examine more details concerning the role and impact that ABL and shallow-cumulus cloud schemes have on short- and medium-range weather forecasting. For instance, another study is currently under way to find out how MoisTKE and Kuo Transient modify the statistical characteristics of

Unauthenticated | Downloaded 08/13/24 05:34 PM UTC

precipitation (e.g., probability density functions, spectral properties) for a summertime heavy precipitation event over land.

It should be mentioned, at this point, that the multischeme approach presented in this study was shown to be appropriate for this particular configuration and application of GEM. In other atmospheric models, in which other cloud schemes are included, it may not be necessary to have four different parameterization schemes to represent the wide variety of clouds that were observed in the large-scale system examined in this study. Also, it is not clear at what scales or model resolutions the boundary layer and shallow cloud schemes become unnecessary. Further investigations on the necessity of using this type of subgrid-scale cloud schemes in very high resolution mesoscale models (e.g., 1-km grid spacing) are underway.

Finally, it is worth pointing out that the multischeme configuration described in this study has been recently implemented in the regional version of GEM used operationally at CMC for short-range weather forecasting, and that it is on the verge of being proposed for the global medium-range version of GEM.

Acknowledgments. SSM/I images were generated using data produced by Remote Sensing Systems and sponsored by the NASA Pathfinder Program for Earth Observing Systems (EOS) products. We thank Gérard Pellerin (CMC) for his contribution to the Kuo Transient scheme. We are also grateful to Michel Roch (MRB) and Anne-Marie Leduc (CMC) for all the work they have done on the global mesoscale version of GEM. We wish to acknowledge the contribution of Serge Trudel (CMC) for his help with AVHRR images. We also wish to mention our appreciation of the useful discussions with Jean-François Mahfouf (MRB), André Tremblay (MRB), Bernard Bilodeau (MRB), and Michael Desgagné (MRB). Finally, we thank the two anonymous reviewers who helped improve the quality of this work.

REFERENCES

Anthes, R. A., 1977: A cumulus parameterization scheme utilizing a one-dimensional cloud model. *Mon. Wea. Rev.,* **105,** 270–286.

Austin, P. H., M. B. Baker, A. M. Blyth, and J. B. Jensen, 1985: Small-scale variability in warm continental cumulus clouds. *J. Atmos. Sci.,* **42,** 1123–1138.

——, Y. Wang, R. Pincus, and V. Kujala, 1995: Precipitation in stratocumulus clouds: Observational and modeling results. *J. Atmos. Sci.,* **52,** 2329–2352.

Bechtold, P., and P. Siebesma, 1998: Organization and representation of boundary layer clouds. *J. Atmos. Sci.,* **55,** 888–895.

——, C. Fravalo, and J. P. Pinty, 1992: A model of marine boundary-layer cloudiness for mesoscale applications. *J. Atmos. Sci.,* **49,** 1723–1744.

——, J. W. M. Cuijpers, P. Mascart, and P. Trouilhet, 1995: Modeling of trade wind cumuli with a low-order turbulence model: Toward a unified description of Cu and Sc clouds in meteorological models. *J. Atmos. Sci.,* **52,** 455–463.

Bélair, S., J. Mailhot, J. W. Strapp, and J. I. MacPherson, 1999: An examination of local versus nonlocal aspects of a TKE-based boundary layer scheme in clear convective conditions. *J. Appl. Meteor.,* **38,** 1499–1518.

——, A. Méthot, J. Mailhot, B. Bilodeau, A. Patoine, G. Pellerin, and J. Côté, 2000: Operational implementation of the Fritsch–Chappell convective scheme in the 24-km Canadian regional model. *Wea. Forecasting,* **15,** 257–274.

——, R. Brown, J. Mailhot, B. Bilodeau, and L.-P. Crevier, 2003a: Operational implementation of the ISBA land surface scheme in the Canadian regional weather forecast model. Part II: Cold season results. *J. Hydrometeor.,* **4,** 371–386.

——, L.-P. Crevier, J. Mailhot, B. Bilodeau, and Y. Delage, 2003b: Operational implementation of the ISBA land surface scheme in the Canadian regional weather forecast model. Part I: Warm season results. *J. Hydrometeor.,* **4,** 352–370.

Benoit, R., J. Côté, and J. Mailhot, 1989: Inclusion of a TKE boundary layer parameterization in the Canadian regional finite-element model. *Mon. Wea. Rev.,* **117,** 1726–1750.

Blyth, A. M., 1993: Entrainment in cumulus clouds. *J. Appl. Meteor.,* **32,** 626–641.

Bougeault, P., 1981: Modeling the trade-wind cumulus boundary layer. Part I: Testing the ensemble cloud relations against numerical data. *J. Atmos. Sci.,* **38,** 2414–2428.

——, 1985a: The diurnal cycle of the marine stratocumulus layer: A higher-order model study. *J. Atmos. Sci.,* **42,** 2826–2843.

——, 1985b: A simple parameterization of the large-scale effects of cumulus convection. *Mon. Wea. Rev.,* **113,** 2108–2121.

——, and P. Lacarrère, 1989: Parameterization of orography-induced turbulence in a mesobeta-scale model. *Mon. Wea. Rev.,* **117,** 1872–1890.

Brenguier, J. L., and Coauthors, 2000: An overview of the ACE-2 CLOUDYCOLUMN closure experiment. *Tellus,* **52B,** 815–827.

Chaboureau, J.-P., and P. Bechtold, 2002: A simple cloud parameterization derived from cloud resolving model data: Diagnostic and prognostic applications. *J. Atmos. Sci.,* **59,** 2362–2372.

Chlond, A., 1992: Three-dimensional simulation of cloud street development during a cold air outbreak. *Bound.-Layer Meteor.,* **58,** 161–200.

Côté, J., J.-G. Desmarais, S. Gravel, A. Méthot, A. Patoine, M. Roch, and A. Staniforth, 1998a: The operational CMC–MRB global environmental multiscale (GEM) model. Part II: Results. *Mon. Wea. Rev.,* **126,** 1397–1418.

——, S. Gravel, A. Méthot, A. Patoine, M. Roch, and A. Staniforth, 1998b: The operational CMC–MRB global environmental multiscale (GEM) model. Part I: Design considerations and formulation. *Mon. Wea. Rev.,* **126,** 1373–1395.

Cuijpers, J. W. M., and P. Bechtold, 1995: A simple parameterization of cloud water related variables for use in boundary layer models. *J. Atmos. Sci.,* **52,** 2486–2490.

——, P. G. Duynkerke, and F. T. M. Nieuwstadt, 1996: Analyses of variance and flux budgets in cumulus-topped boundary layers. *Atmos. Res.,* **40,** 307–337.

Unauthenticated | Downloaded 08/13/24 05:34 PM UTC

Deardorff, J. W., 1980: Cloud top entrainment instability. *J. Atmos. Sci.,* **37,** 131–147.

Deng, A., N. L. Seaman, and J. S. Kain, 2003: A shallow-convection parameterization for mesoscale models. Part I: Submodel description and preliminary applications. *J. Atmos. Sci.,* **60,** 34–56.

de Roode, S. R., and P. G. Duynkerke, 1997: Observed Lagrangian transition of stratocumulus into cumulus during ASTEX: Mean state and turbulence structure. *J. Atmos. Sci.,* **54,** 2157–2173.

Driedonks, A. G. M., and P. G. Duynkerke, 1989: Current problems in the stratocumulus-topped atmospheric boundary layer. *Bound.-Layer Meteor.,* **46,** 275–303.

Duynkerke, P. G., and A. G. M. Driedonks, 1987: A model for the turbulent structure of the stratocumulus-topped atmospheric boundary layer. *J. Atmos. Sci.,* **44,** 43–64.

——, and ——, 1988: Turbulent structure of a shear-driven stratus-topped atmospheric boundary layer: A comparison of model results with observations. *J. Atmos. Sci.,* **45,** 2343–2351.

——, H. Zhang, and P. J. Jonker, 1995: Microphysical and turbulent structure of nocturnal stratocumulus as observed during ASTEX. *J. Atmos. Sci.,* **52,** 2763–2777.

Fouquart, Y., and B. Bonnel, 1980: Computations of solar heating of the earth's atmosphere: A new parameterization. *Contrib. Atmos. Phys.,* **53,** 35–62.

Garand, L., 1983: Some improvements and complements to the infrared emissivity algorithm including a parameterization of the absorption in the continuum region. *J. Atmos. Sci.,* **40,** 230–244.

Golaz, J.-C., V. E. Larson, and W. R. Cotton, 2002: A PDF-based model for boundary layer clouds. Part I: Method and model description. *J. Atmos. Sci.,* **59,** 3540–3551.

Kain, J., and J. M. Fritsch, 1990: A one-dimensional entraining/detraining plume model and its application in convective parameterization. *J. Atmos. Sci.,* **47,** 2784–2802.

——, and ——, 1993: Convective parameterization for mesoscale models: The Kain–Fritsch scheme. *The Representation of Cumulus Convection in Numerical Models, Meteor. Monogr.,* No. 46, Amer. Meteor. Soc., 165–170.

Kuo, H. L., 1965: On formation and intensification of tropical cyclones through latent heat release by cumulus convection. *J. Atmos. Sci.,* **22,** 40–63.

——, 1974: Further studies on the parameterization of the influence of cumulus convection on large-scale flow. *J. Atmos. Sci.,* **31,** 1232–1240.

Lappen, C.-L., and D. A. Randall, 2001: Toward a unified parameterization of the boundary layer and moist convection. Part I: A new type of mass-flux model. *J. Atmos. Sci.,* **58,** 2021–2036.

Lewellen, D. C., W. S. Lewellen, and S. Yoh, 1996: Influence of Bowen ratio on boundary-layer cloud structure. *J. Atmos. Sci.,* **53,** 175–187.

Louis, J.-F., Ed., 1984: ECMWF forecast model physical parameterization research manual 3. European Centre for Medium-Range Weather Forecasts, Reading, United Kingdom, 56 pp.

Mailhot, J., and S. Bélair, 2002: An examination of a unified cloudiness-turbulence scheme with various types of cloudy boundary layers. Preprints, *15th Conf. on Boundary Layer and Turbulence*, Wageningen, Netherlands, Amer. Meteor. Soc., 215–218.

——, and Coauthors, 1998: Scientific description of RPN physics library. Recherche en Prévision Numérique, version 3.6, 188 pp. [Available from RPN, 2121 Trans-Canada, Dorval, PQ H9P 1J3, Canada. Also available online at http://www.smc-msc.ec.gc.ca/cmc_library/index_e.html.]

Malkus, J. S., 1954: Some results of a trade-cumulus cloud investigation. *J. Meteor.,* **11,** 220–237.

Molinari, J., and M. Dudek, 1992: Parameterization of convective precipitation in mesoscale numerical models: A critical review. *Mon. Wea. Rev.,* **120,** 326–344.

Nicholls, S., 1984: The dynamics of stratocumulus: Aircraft observations and comparisons with a mixed layer model. *Quart. J. Roy. Meteor. Soc.,* **110,** 783–820.

Pudykiewicz, J., R. Benoit, and J. Mailhot, 1992: Inclusion and verification of a predictive cloud water scheme in a regional weather prediction model. *Mon. Wea. Rev.,* **120,** 612–626.

Randall, D. A., 1980a: Entrainment into a stratocumulus layer with distributed radiative cooling. *J. Atmos. Sci.,* **37,** 148–159.

——, 1980b: Conditional instability of the first kind upside-down. *J. Atmos. Sci.,* **37,** 125–130.

——, 1984: Stratocumulus cloud deepening through entrainment. *Tellus,* **36A,** 446–457.

Riehl, H., T. C. Yeh, J. S. Malkus, and N. E. La Seur, 1951: The north-east trade of the Pacific Ocean. *Quart. J. Roy. Meteor. Soc.,* **77,** 598–626.

Siebesma, A. P., 1998: Shallow cumulus convection. *Buoyant Convection in Geophysical Flows,* E. J. Plate et al., Eds., Kluwer Academic, 441–486.

Slingo, A., R. Brown, and C. L. Wrench, 1982a: A field study of nocturnal stratocumulus. III. High resolution radiative and microphysical observations. *Quart. J. Roy. Meteor. Soc.,* **108,** 145–165.

——, S. Nicholls, and J. Schmetz, 1982b: Aircraft observations of marine stratocumulus during JASIN. *Quart. J. Roy. Meteor. Soc.,* **108,** 833–856.

Slingo, J. M., 1987: The development and verification of a cloud prediction scheme for the ECMWF model. *Quart. J. Roy. Meteor. Soc.,* **113,** 899–927.

Sommeria, G., 1976: Three-dimensional simulation of turbulent processes in an undisturbed trade wind boundary layer. *J. Atmos. Sci.,* **33,** 216–241.

——, and J. W. Deardorff, 1977: Subgrid-scale condensation in models of nonprecipitating clouds. *J. Atmos. Sci.,* **34,** 344–355.

Stevens, B., 2002: Entrainment in stratocumulus-topped mixed layers. *Quart. J. Roy. Meteor. Soc.,* **128,** 2663–2690.

——, W. R. Cotton, G. Feingold, and C.-H. Moeng, 1998: Large-eddy simulations of strongly precipitating, shallow, stratocumulus-topped boundary layers. *J. Atmos. Sci.,* **55,** 3616–3638.

——, and Coauthors, 2003: Dynamics and chemistry of marine stratocumulus—DYCOMS-II. *Bull. Amer. Meteor. Soc.,* **84,** 579–593.

Stull, R. B., 1985: A fair-weather cumulus cloud classification scheme for mixed-layer studies. *J. Climate Appl. Meteor.,* **24,** 49–56.

——, 1988: *An Introduction to Boundary Layer Meteorology.* Kluwer Academic, 666 pp.

Sundqvist, H., 1978: A parameterization scheme for non-convective condensation including prediction of cloud water content. *Quart. J. Roy. Meteor. Soc.,* **104,** 677–690.

——, 1993: Inclusion of ice phase of hydrometeors in cloud parameterization for mesoscale and large scale models. *Contrib. Atmos. Phys.,* **66,** 137–147.

Unauthenticated | Downloaded 08/13/24 05:34 PM UTC

Taylor, G. R., and M. B. Baker, 1991: Entrainment and detrainment in cumulus clouds. *J. Atmos. Sci.,* **48,** 112–121.

Teixeira, J., and T. F. Hogan, 2002: Boundary layer clouds in a global atmospheric model: Simple cloud cover parameterizations. *J. Climate,* **15,** 1261–1276.

Tiedtke, M., 1989: A comprehensive mass flux scheme for cumulus parameterization in large-scale models. *Mon. Wea. Rev.,* **117,** 1779–1800.

——, 1993: Representation of clouds in large-scale models. *Mon. Wea. Rev.,* **121,** 3040–3061.

von Salzen, K., and N. McFarlane, 2002: Parameterization of the bulk effects of lateral and cloud-top entrainment in transient shallow cumulus clouds. *J. Atmos. Sci.,* **59,** 1405–1430.

Wang, Q., and D. H. Lenschow, 1995: An observational study of the role of penetrating cumulus in a marine stratocumulus-topped boundary layer. *J. Atmos. Sci.,* **52,** 2778–2787.

Zhang, D.-L., J. S. Kain, J. M. Fritsch, and K. Gao, 1994: Comments on "Parameterization of convective precipitation in mesoscale numerical models: A critical review." *Mon. Wea. Rev.,* **122,** 2222–2231.

Unauthenticated | Downloaded 08/13/24 05:34 PM UTC